# Spreading of Levantine Intermediate Waters by submesoscale coherent vortices in the northwestern Mediterranean Sea as observed with gliders

Anthony Bosse, Pierre Testor, Laurent Mortier, Louis Prieur, Vincent Taillandier, Fabrizio D'Ortenzio, Laurent Coppola

AGU PUBLICATIONS

JGR

Journal of Geophysical Research: Oceans

RESEARCH ARTICLE

10.1002/2014JC010263

**Key Points:**
- Submesoscale eddies of warm/salty intermediate waters were revealed by gliders
- The eddies are very energetic and coherent structures that can live for months
- The eddies have likely strong implications for the physics of the NW Mediterranean Sea

**Correspondence to:**
A. Bosse,
bosse@locean-ipsl.upmc.fr

**Citation:**
Bosse, A., P. Testor, L. Mortier, L. Prieur, V. Taillandier, F. d'Ortenzio, and L. Coppola (2015), Spreading of Levantine Intermediate Waters by submesoscale coherent vortices in the northwestern Mediterranean Sea as observed with gliders, *J. Geophys. Res. Oceans*, *120*, doi:10.1002/2014JC010263.

Received 24 JUN 2014
Accepted 6 FEB 2015
Accepted article online 12 FEB 2015

# Spreading of Levantine Intermediate Waters by submesoscale coherent vortices in the northwestern Mediterranean Sea as observed with gliders

**Anthony Bosse[1], Pierre Testor[1], Laurent Mortier[2], Louis Prieur[3], Vincent Taillandier[3], Fabrizio d'Ortenzio[3], and Laurent Coppola[3]**

[1]Sorbonne Universités, UPMC Univ. Paris 06-CNRS-IRD-MNHN, UMR 7159, Laboratoire d'Océanographie et du Climat, IPSL, Paris, France, [2]ENSTA–Paristech, Palaiseau, France, [3]Sorbonne Universités, UPMC Univ. Paris 06, UMR 7093, LOV, Observatoire Océanologique, Villefranche/mer, France

**Abstract** Since 2007, gliders have been regularly deployed in the northwestern Mediterranean Sea, a crucial region regarding the thermohaline circulation of the Mediterranean Sea. It revealed for the first time very warm (+0.4°C) and saline (+0.1) submesoscale anticyclones at intermediate depth characterized by a small radius (∼5 km), high Rossby (∼0.3), and Burger (∼0.7) numbers. They are likely order of 10 to be formed each year, have a life time order a year and certainly contribute significantly to the spreading of the Levantine Intermediate Waters (LIW) toward the whole subbasin, thus potentially impacting wintertime vertical mixing through hydrographical and dynamical preconditioning. They could be mainly formed by the combined action of turbulent mixing and flow detachment of the northward flow of LIW at the northwestern headland of Sardinia. Upwelling conditions along the western coast of Sardinia associated with a southward geostrophic flow within the upper layers seem to play a key role in their formation process.

## 1. Introduction

The Levantine Intermediate Water (LIW) is a water mass formed in the eastern Mediterranean Sea by combined effects of evaporation increasing salinity in Summer and relatively deep vertical mixing caused by intense dry northerly winds in Winter [*Lascaratos et al.*, 1999]. After reaching its equilibrium depth, the LIW flows at mid depths (200–500 m) and enters the western Mediterranean Sea and the Tyrrhenian Sea partly cascading through the channel of Sicily-Tunisia (sill at around 400 m) [*Millot*, 1999]. It eventually reaches the westernmost subbasins through the channel of Sardinia-Tunisia (sill at around 2000 m) and, to a lower extent, through the strait of Corsica (shallower sill at about 400 m depth), see Figure 1.

The LIW follows a cyclonic circulation in the western subbasins [*Millot*, 1999]. It takes the form of a northward vein along the continental slope of Sardinia [*Millot*, 1987]. It then flows further downstream with the Western Corsica Current (WCC) and the Northern Current (NC), see black arrows in Figure 1. Its hydrographic characteristics are modified all along its path following the continental slope, through cross-shelf exchanges. This LIW flow is already known to be subjected to sporadic spreading toward the Algerian basin. This can be due to filaments swirling around "Algerian Eddies" (AEs) interacting with the LIW vein [*Millot and Taupier-Letage*, 2005]. In addition, *Testor and Gascard* [2005] found evidences of flow detachment by the formation of the barotropic "Sardinian Eddies" (SEs). They were found to accumulate South of the North-Balearic Front (NBF), a dynamical barrier between the southern and northern subbasins [see *Mancho et al.*, 2008 for a numerical study of the surface circulation], before being sooner or later entrained southward by the Algerian Gyres (the general circulation of this subbasin) [*Testor et al.*, 2005b].

Contrary to the Algerian basin, no process involved in the spreading of the LIW toward the interior of the northwestern Mediterranean Sea (NWMed) has been clearly identified up to now. Though, the physics of the NWMed is of critical importance for the thermohaline circulation of the Mediterranean Sea [*Robinson and Golnaraghi*, 1994] and its outflow into the Atlantic Ocean at the Strait of Gibraltar [*Stommel et al.*, 1973].

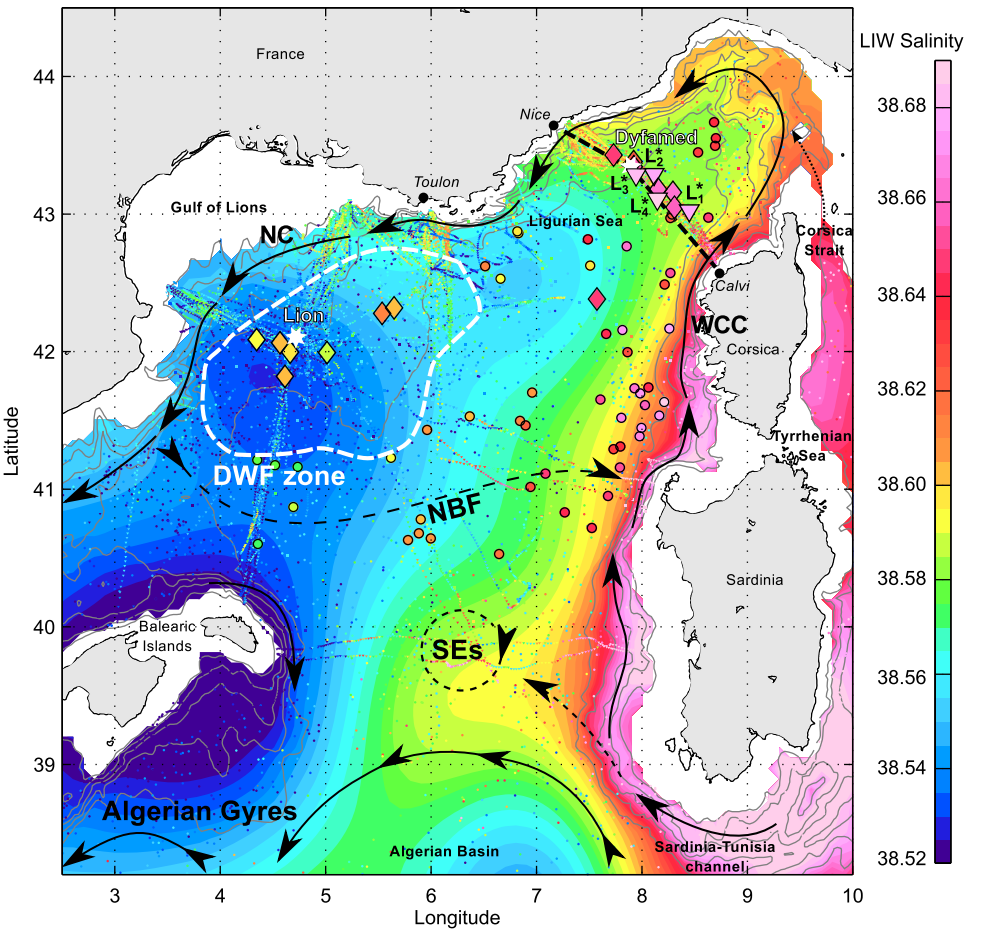


**Figure 1.** Objectively analyzed map of the LIW salinity from observations carried out in the January 2007 to August 2013 period. Small markers represent all the individual profiles collected by gliders, shipborne CTD casts, and Argo floats. Large inverted triangle represent the glider observations of LIW SCVs with the strongest $\theta/S$ signature ($L_i^*$), and large diamond with less marked ones ($L_i$ in the Ligurian Sea and $G_i$ in the Gulf of Lions). Contoured circles are Argo or CTD profiles north of 40°N30′ with a positive LIW salinity anomaly greater than 0.04 ($\sim 2\times \mathrm{std}_{S'}$, with $\mathrm{std}_{S'}$ the standard deviation of the differences between the observations and the analyzed LIW salinity field). All markers are colored according to their LIW salinity. The dashed black line indicates the Nice-Calvi section repeatedly carried out by gliders. Arrows with continuous line represent the mean currents (NC: Northern Current, WCC: Western Corsica Current, NBF: North Balearic Front) found at intermediate depths (under 300 m depth), and arrows with dashed lines other important circulation features (SEs: Sardinian Eddies). The Deep Water Formation (DWF) area is highlighted by the white-dashed line. Dyfamed and Lion are the two moorings used for the calibration of the gliders and the Argo floats. Isobaths are also depicted every 500 m.

The Gulf of Lions area is indeed the main place in the western Mediterranean Sea, and one of the few places of the world's oceans, where open ocean deep convection can occur [*Marshall and Schott*, 1999]. These phenomena renew the Western Mediterranean Deep Waters (WMDW) [*MEDOC-Group*, 1970] and the LIW plays a key role in this process by storing heat and salt at intermediate depths, which then affects the depth of the deep convection and the hydrological properties of the water mass that can be formed [*Lacombe et al.*, 1985; *Grignon et al.*, 2010]. On average, WMDW are presently characterized by a potential temperature of $\sim$ 12.86–12.89°C and a salinity $\sim$ 38.48–38.50 below 1000 m depth [*Houpert*, 2013].

In this study, we shed some light on the crucial question of the spreading of the LIW toward the NWMed thanks to the glider technology [*Testor et al.*, 2010]. Gliders regularly crossed the oceanic basin since 2007 and revealed the presence of isolated submesoscale anticyclones with a strong signature in the LIW layer (see an example in Figure 2). Because of their small size, they could have hardly been observed and identified as such by other sampling platforms. We first characterize the LIW salinity variability in the Ligurian Sea before analysing the observed eddies in terms of thermohaline anomalies, origin, and dynamical properties. At last, we discuss their formation process and their implications for the physics (with consequences on the biogeochemistry) of the basin.

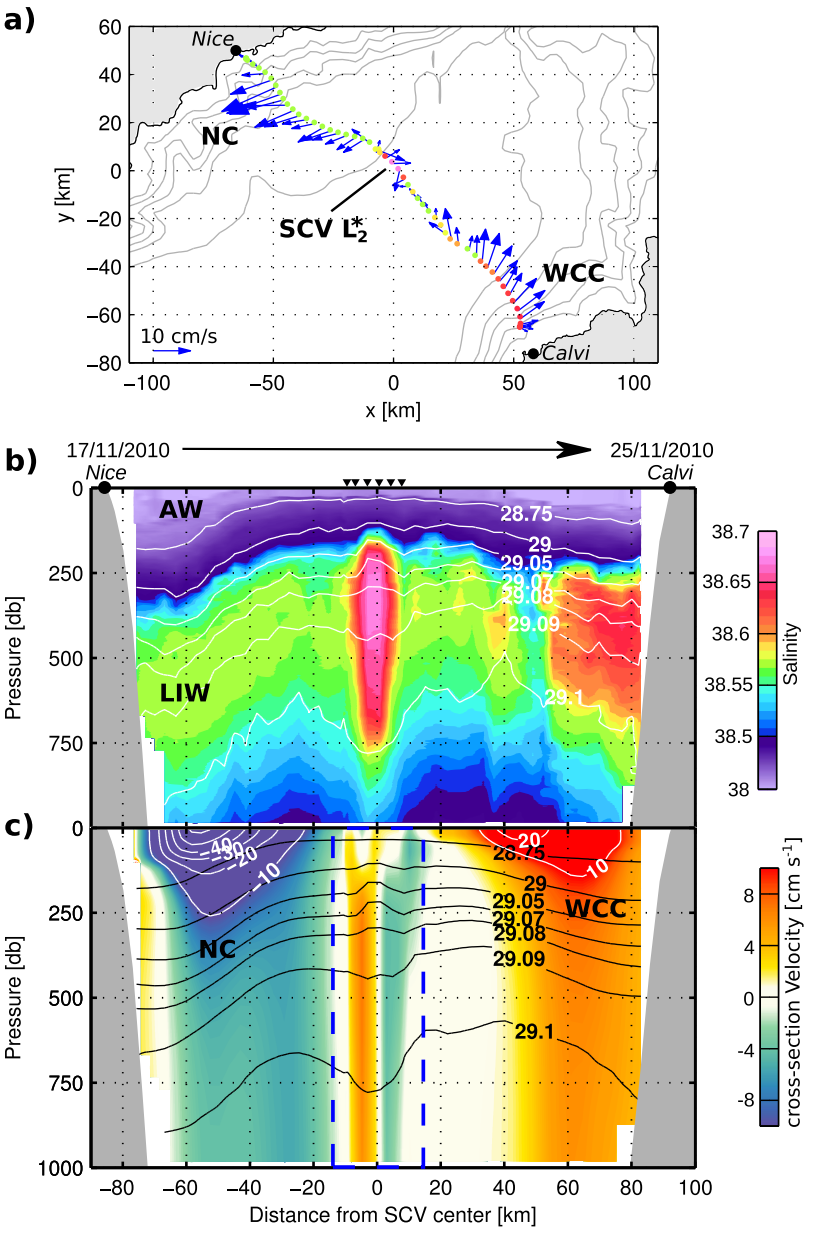


**Figure 2.** A "Nice-Calvi" glider section in November 2010 revealing the presence of the SCV $L_2^*$: (a) Glider pathway from Nice to Calvi with the LIW salinity of each profile colored according to the colorbar of (b) and depth-average currents deduced by the glider. The path of the NC and the WCC is also shown. (b) Salinity section with density contours in white. Black triangles show the position of glider profiles carried out within the SCV. (c) Cross-section velocities (cyclostrophic within the blue box and geostrophic outside) with contours in cm $s^{-1}$. The black contours show the smoothed density field. As stated in the text, the smoothing is performed with L = 2 km between the dashed blue lines. Outside, the width of the Gaussian function is taken slightly larger (L = 5 km) since the boundary currents (the Northern Current (NC) and the Western Corsica Current (WCC)) are associated with larger horizontal scales.

## 2. Data and Methods

### 2.1. Hydrographical Data Set

The very first glider deployments in the NWMed were carried out in 2006. In 2010, gliders started to be deployed on a regular basis in the framework of MOOSE (Mediterranean Ocean Observing System for the Environment, http://www.moose-network.fr/). In this study, we use a data set composed of all profiles carried out by gliders from 2007 to August 2013 in the NWMed (more than 25,000 profiles down to 1000 m), as well as about 400 shipborne CTD casts collected by R/V and about 2500 Argo profiles collected during the same period flagged as "good" by the Coriolis Data Center (http://www.coriolis.eu.org/). A first-order

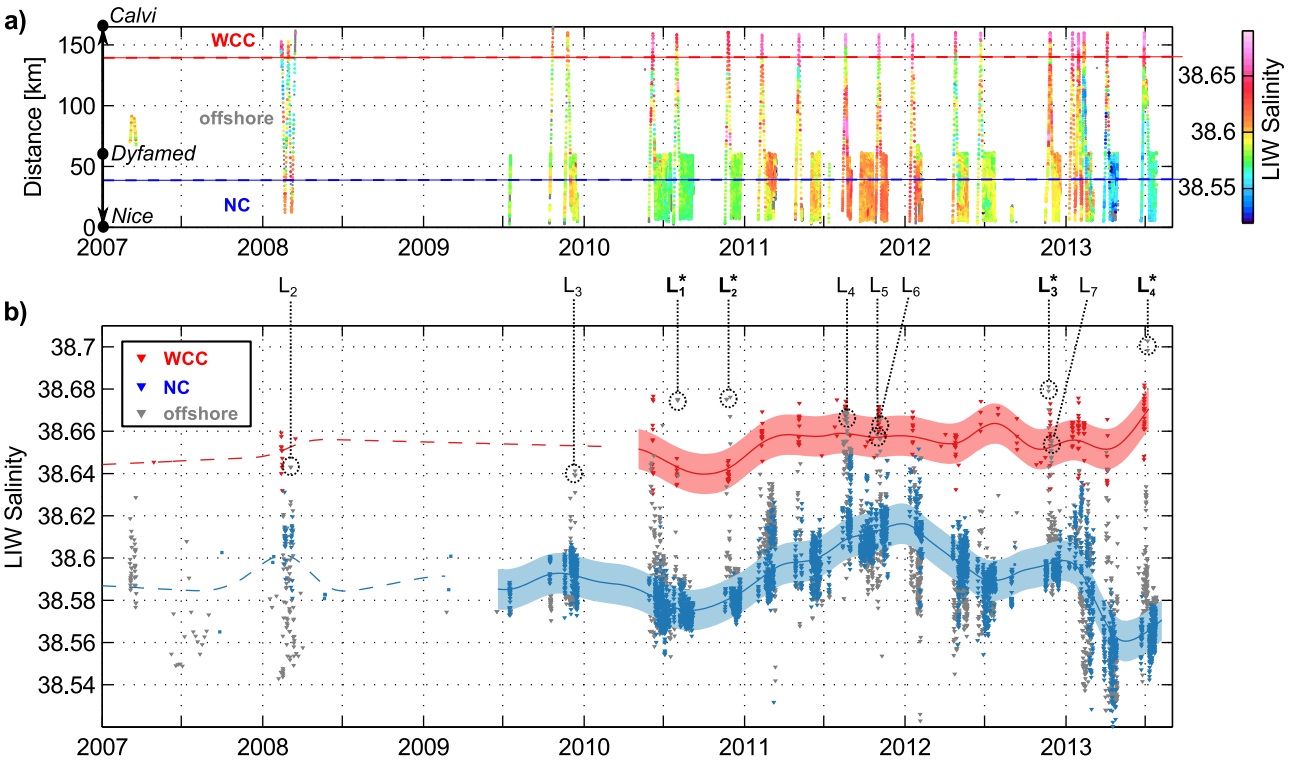


**Figure 3.** (a) Hovmöller diagram of the LIW salinity observed along the Nice-Calvi section. (b) Temporal evolution of the LIW salinity offshore (gray dots) and within the two boundary currents: the NC in blue ($d < 40$ km) and the WCC in red ($d > 140$ km). The red and blue lines are the low-pass filtered signals associated with time scale larger than 3 months. Positive salinity anomalies associated with LIW SCVs are labeled.

consistency (offset correction) of the data set is achieved by profile to profile comparison in the deep layers ($>$ 700 m) of the gliders and the Argo floats data with reference to in laboratory-calibrated CTD casts (Seabird SBE 911+), as well as two moorings operated since 2007 (LION: 11 Seabird microcats from 100 to 2300 m [*Houpert*, 2013], and DYFAMED: 2 Seabird microcats at 700 and 1000 m, the location of the moorings is shown in Figure 1), and a final cross-calibration step (within intervals of 5 days and 15 km). The absolute values of computed offsets were on average about 0.01°C and 0.01 in salinity. We checked the consistencies in the deep layers ($>$ 700 m), where the variance of the temperature and salinity are relatively small. At these depths, the variability is indeed significantly smaller ($\text{std}_\theta = 0.0002$°C and $\text{std}_S = 0.003$) and allows to determine a general offset for each sensor. This can be optimized but is relative, and the overall consistency of the data set is provided by the calibrated CTD data from the MOOSE research cruises (ground truth).

Particular attention is given to glider deployments revealing the presence of similar interesting circulation features. Temperature and salinity collected by these gliders were carefully compared at depths greater than 700 m with nearby CTD casts collected by R/V and calibrated mooring data at LION or DYFAMED allowing to keep the glider CTD biases in temperature and salinity smaller than, respectively, 0.01°C and 0.01.

From September 2009 to August 2013, gliders carried out 35 Nice-Calvi sections (location shown in Figure 1) on a regular basis with a sampling down to 1000 m, and many more shorter transects from Nice to DYFAMED with a sampling restricted to the upper 500 m (see Figure 3a). The density of observations is particularly important along the Nice-Calvi section compared to anywhere else in the NWMed. This enables a detailed inspection of the LIW properties flowing in the Northern Current and in the Western Corsica Current during this 4 years period. From these data, some aspects of the seasonal and interannual variability can be discussed.

Gliders sample the ocean along a sawtooth trajectory between the surface and a maximum depth of 1000 m. As the slopes of isopycnals are much smaller than the pitch angle of the glider (about $\pm 25$°), the glider dives and ascents can be considered as vertical profiles. Two profiles to 1000 m are then separated

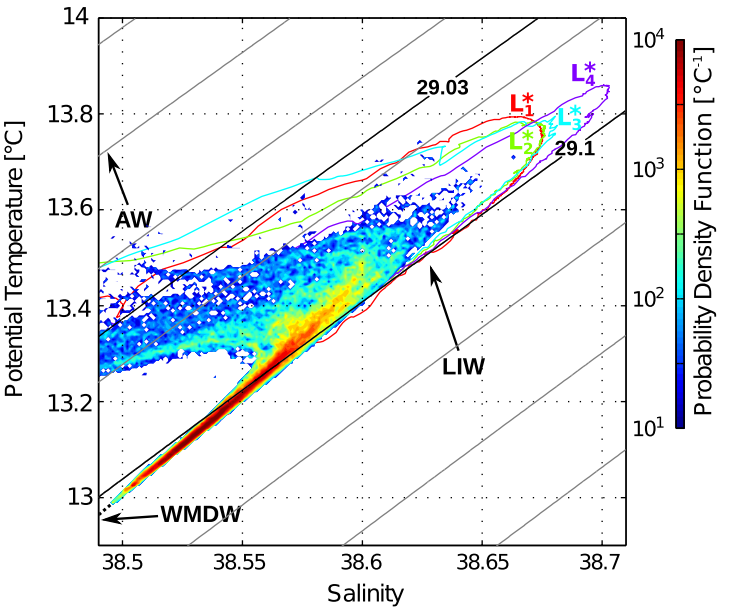


**Figure 4.** Volumetric $\theta/S$ diagram with the main water masses (AW, LIW, and WMDW) made up by all the profiles (down to 1000 m) collected during the four glider deployments revealing the SCV $L_i^*$. The empirical probability density function was normalized such as its integral in the $\theta/S$ space equals to unity. The colored lines labeled by $L_i^*$ are associated with the profiles carried out within the core of the four SCVs. Slanted lines represent isopycnals.

by about 2–4 km and 2–4 h depending on the currents and the sampling strategy (dives only, or dives/ascents). Having a horizontal speed of 30–40 km day$^{-1}$ relative to the water, gliders are perfectly suited to sample oceanic features and eddies that propagate slower. From its dead reckoning navigation and GPS fixes at surface, the glider also deduces a mean current, which is averaged over each dive (hereafter referred as the depth-average currents). Thermal lag issues of the gliders CTD probe were corrected by applying the method of *Garau et al.* [2011].

Argo floats are autonomous profiling floats that drift at a given parking depth for a given time period. By the end of this drifting time, they dive to 2000 m (sometimes 1000 m) and collect during the upcast a profile of temperature and salinity. The data are then sent in real time to the Coriolis data center before the floats eventually return to their parking depth. The MedArgo program set the interval between successive surfacing of Argo floats to 4–5 days and a parking depth of about 400 m at the approximate depth of the LIW layer.

We also used meteorological forecasts of the European Center for Medium-range Forecasts (ECMWF) for the 2007–2011 period and Sea Surface Temperature (SST) images provided by ACRI-ST–Globcolor. This product is based on the combined use of the OSTIA product and SST AVHRR images to improve the spatial resolution of the OSTIA product.

### 2.2. Objective Analysis of the LIW Properties

We defined the basic hydrographical properties of the LIW as the maximum of salinity (S) and potential temperature ($\theta$) measured between two potential density values (29.03 kg m$^{-3} < \sigma_0 <$ 29.10 kg m$^{-3}$) encompassing both temperature and salinity maxima characterizing the LIW layer (see Figure 4). LIW potential temperature (resp. salinity) will hereafter refer to this potential temperature (resp. salinity) maximum, and is considered only for profiles reaching the minimum density of $\sigma_0 = 29.07$ kg m$^{-3}$ required to correctly sample the LIW layer.

From the previously described data set, we aim to describe a basin-scale mean repartition of the LIW salinity that is representative of the last 5 years (88% of the data are posterior to August 2008). To this end, we objectively analyzed the LIW salinity over the whole basin. We first averaged the LIW salinity within $0.1^\circ \times 0.1^\circ$ boxes, and then analyzed this mean field using the method of *Boehme and Send* [2005] with a covariance function conditional to the topography and the planetary vorticity in order to better account for the topographic constraints of the mean flow. We chose $\lambda_s \sim 200$ km and $\Phi = 1$ for the scaling parameters, which corresponds to a Gaussian covariance with a spatial scale of 200 km away from the influence of topography, and means that a factor of four in the difference in $f/h$ ($f$ being the Coriolis parameter and $h$ the bottom depth) contributes to the distance approximately like 200 km separation in space. This spatial correlation scale is typical of the subbasins size, which is consistent with the large-scale variability we want to emphasize.

### 2.3. Reconstruction of the Geostrophic Velocities

From the gliders data, a density section combined with the depth-average currents enables to get a picture of the cross-track geostrophic velocities.

First, a low-pass filter is applied to horizontally smooth the density section with a cutoff length-scale typical of the internal deformation radius, the horizontal scale at which geostrophy can be considered as valid. This is done in order to remove the undesirable effects of unbalanced signal mainly related to internal waves, as shown by *Todd et al*. [2009]. We performed a modal decomposition on 79 full-depth shipborne CTD casts of the previously described observational data set collected in the Ligurian Sea at a bottom depth $>$ 2200 m (longitude $>$ 7°E and latitude $>$ 42°N). We found a first baroclinic deformation radius of 5.6 $\pm$ 0.9 km. This scale is relatively small compared to other oceans owing to the low stratification of the NWMed. We then transform the density section ($\sigma_0$) into a smoothed density section ($\tilde{\sigma_0}$) by using a Gaussian moving average with a significant width of the order of this deformation radius:

$$\tilde{\sigma_0}(r,z)=\int_{r_{min}}^{r_{max}} \sigma_0(r',z)\times e^{-(r'-r)^2/2L^2}dr' \quad (1)$$

where $r$ is the along-section distance, $r_{min}$ and $r_{max}$ the boundaries of the glider section, $z$ the depth and $L$ the standard deviation of the Gaussian function. Setting L equal to 2 km is sufficient to filter out small-scale isopycnal oscillations without fading the dynamical density signature associated with submesoscale anticyclonic eddies, as shown in Figure 2c.

We then solved the geostrophic balance ($v_g$) by vertically integrating the thermal wind balance on the smoothed density section [*Todd et al*., 2009; *Pietri et al*., 2013; *Høydalsvik et al*., 2013] and by taking as a reference for the 0–1000 m mean velocities the cross-section component of the depth-average currents deduced by the gliders. In doing so, it provides also an information on the barotropic component of the flow and enables to get an idea of the "absolute" currents orthogonal to the glider section [*Gourdeau et al*., 2008; *Todd et al*., 2009; *Bouffard et al*., 2010; *Davis et al*., 2012; *Pietri et al*., 2013; *Høydalsvik et al*., 2013; *Pietri et al*., 2014].

## 3. Results

### 3.1. Submesoscale Coherent Vortices of LIW

#### 3.1.1. Mean Distribution of the LIW Salinity at the Basin-Scale

The Figure 1 presents the analyzed map of the LIW salinity. It clearly shows the northward LIW flow along the Sardinian continental slope characterized by high LIW salinities ($\sim$ 38.68–38.70), high horizontal salinity gradients with the open-ocean ($\Delta S \sim$ 0.10 over O(20 km)) and a downstream erosion in terms of salinity characteristics. At the basin-scale, a weak east-west salinity gradient can be observed ($\Delta S \sim -0.05$ over O(200 km)). The lowest values of the LIW salinity of the NWMed are found in the Gulf of Lions ($\sim$ 38.54), where the WMDW are formed. Indeed, the recurrent wintertime deep vertical mixing often mix the LIW layer with the fresher waters lying above and below it. It thus lowers the mean salt content of the LIW layer in that area. Between the Balearic Islands and Sardinia, relatively high LIW salinities ($\sim$ 38.59) are also observed. This can be the result of the generation of the Sardininan Eddies that can transport salt from the Sardinian continental slope to the open ocean region located south of the NBF [*Testor et al*., 2005a, 2005b].

The LIW salinity of each profile used to build up the objectively analyzed map is superimposed in the Figure 1 using the same color scale. So contrasted markers are indicating local deviations to the large-scale analyzed field. The open ocean observations then reveal a high variability, often higher than the standard deviation of the observations minus the objectively analyzed LIW salinity field which is $\sim$ 0.02 and this implies the presence of ubiquitous turbulent features. Numerous positive salinity anomalies are found offshore and the eddies described in the following are associated with the strongest anomalies one can find over the whole studied area.

#### 3.1.2. LIW Variability in the Ligurian Sea

We can distinguish three zones along the Nice-Calvi section according to $d$ the distance to the French coast, as illustrated by the Figure 1 showing the main circulation of the basin: the NC area ($d <$ 40 km), the WCC area close to Corsica ($d >$ 140 km), and in between the offshore area (see Figure 3, top). The boundaries for the NC and the WCC were determined by examining Nice-Calvi sections (see an example with Figure 2) and represent approximately the mean position of the external margin of those two currents. The WCC transports much more saline LIW ($\sim$ 38.66) than the NC ($\sim$ 38.60). In the offshore region, the LIW properties are

more similar to those of the NC with the isolated presence of small salinity anomalies certainly corresponding to turbulent circulation features.

In some years, the NC and offshore areas seem to be driven by a strong seasonal variability (see Figure 3b). In winter, the LIW salinity transported by the NC can decrease by up to 0.04 (especially noticeable during winter 2012 and 2013) compared to prewinter values. In 2013, gliders data very well captured this drop in salinity. This variability has to be related to deep vertical mixing, that can occur offshore during strong wintertime conditions. The mixed layer can indeed reach depths greater than the LIW layer ($>$1000 m measured offshore in February 2013). It also suggests the NC incorporates significant amounts of offshore waters that are in winter directly subjected to intense vertical mixing. These exchanges are likely driven by an enhanced winter mesoscale [*Albérola et al*., 1995] or even submesoscale [*Niewiadomska et al*., 2008] activity of the NC front. Then, from April to the following winter, the LIW salinity progressively increases thanks to the more or less continuous advection of more saline and warm LIW flowing along Sardinia and Corsica (see the circulation pattern in Figure 1). On the contrary, the WCC composed of particularly warm and salty LIW compared to the NC seems to be less subjected to this seasonal forcing.

On interannual timescale, the post winter LIW salinity has recently reached a low value in the NC and the offshore area ($\sim$ 38.56 in April 2013) after two consecutive episodes of strong winter convection. No significant variation of the LIW salinity in the WCC can be noticed apart from a small year-to-year variability and relatively high values observed in June 2013 ($\sim$ 38.68).

#### 3.1.3. Identification of Submesoscale Vortices of LIW

From the data collected along the repeated Nice-Calvi section, we identified in particular four astonishing LIW anomalies of much warmer ($+$0.34–0.51°C) and more saline ($+$0.09–0.14) waters than their direct surroundings (hereafter referred as $L^*_{1-4}$, see Table 1). These profiles reach outstanding LIW hydrographical characteristics compared to the typical values observed offshore, as revealed by the $\theta/S$ diagram of the Figure 4. Furthermore, they all correspond to offshore LIW salinity measurements that even exceed the LIW salinity found within the WCC (see Figure 3b). They are very well pronounced on two to three consecutive profiles surrounded by more ordinary profiles, see Figure 2a. Note that these local anomalies in the LIW hydrographical properties are computed relative to a *far-field* region and not to the climatological LIW salinity field shown by the Figure 1. The *far-field* is defined as the mean of the 10 closest glider profiles found around each anomaly (corresponding to a maximum distance of about 20 km). It is representative of the surrounding waters, which have roughly uniform characteristics, the variability within the *far-field* being one order of magnitude smaller than the anomalies themselves ($\sim$ 0.01 for the LIW salinity and $\sim$ 0.05°C for the LIW potential temperature). It allows a characterization of each $\theta/S$ anomaly with respect to a *background* LIW field excluding such outliers but having some large-scale spatial variability, as well as seasonal, and interannual variability. In the following, we then consider LIW anomalies defined as this difference relative to this *far-field*.

The observation in the open ocean of such marked $\theta/S$ anomalies suggests the presence of dynamical structures (either eddies or filaments) that could be able to transport warm and saline LIW far away from their source. The depth-average currents estimated by the gliders then provide precious informations about the water displacement that can clarify the situation. The distance between two consecutive dives being in average 3.5 km, the high resolution of the glider sampling is therefore sufficient to reveal a potential rotation that could be associated with relatively small eddies (minimum diameter $\sim$ 7 km). We locally removed from the depth-average currents a large-scale mean advection computed by averaging the depth-average currents measured within a given temporal ($\pm$ 1 day) and spatial ($\pm$ 25 km) running window. In some cases, the eddy signal is indeed dominated by an important advection. At last, an anticyclonic rotation was then identifiable around each $\theta/S$ anomaly we identified indicating that they are the signature of small anticyclonic eddies (radius $\sim$ 5–10 km).

The Figure 2 shows a section across the anticyclone $L^*_2$, which has similar characteristics to the other ones. The isopycnal deformation below the thermocline shows a lenticular shape with a doming in the upper part of the LIW core and a lowering of isopycnals below. This is a typical feature of subthermocline Submesoscale Coherent Vortices (SCVs) [*McWilliams*, 1985]. They are characterized by a low-stratified core at intermediate depth below the thermocline. Within this subthermocline core, the potential temperature and salinity are found to be anomalously high and homogeneous compared to classical profiles (Figure 5). No

Journal of Geophysical Research: Oceans

10.1002/2014JC010263

**Table 1.** SCVs Characteristics[a]

| | | $\theta \mid \Delta\theta$ | $S \mid \Delta S$ | d | $\epsilon$ | $R_\epsilon$ | $V_\epsilon^{max}$ | $P@V^{max}$ | $T_r$ | Ro | $N_{scv} \mid N_{out}$ | Bu | $q_{scv}/10^{-12}$ | $\delta q/q$ |
|---|---|---|---|---|---|---|---|---|---|---|---|---|---|---|
| Id | obs. | (°C) | – | (km) | – | (km) | (cm $s^{-1}$) | (m) | (days) | | xf ($s^{-1}$) | | ($m^{-1}$ $s^{-1}$) | % |
| $L_1^*$ | Aug 2010 | 13.79 \| +0.39 | 38.68 \| +0.10 | 2.1 ± 0.5 | 1.07 ± 0.03 | 5.7 ± 1.6 | 6.5 ± 1.3 | 590 ± 80 | 6.4 ± 2.7 | −0.23 ± 0.10 | 6.5 ± 0.6 \| 8.0 ± 0.7 | 0.60 ± 0.26 | 3.3 ± 0.5 | −50 ± 17 |
| $L_2^*$ | Nov 2010 | 13.79 \| +0.36 | 38.68 \| +0.10 | 1.5 ± 0.5 | 1.04 ± 0.02 | 5.5 ± 2.2 | 7.6 ± 1.6 | 430 ± 40 | 5.3 ± 2.6 | −0.28 ± 0.13 | 5.3 ± 0.6 \| 6.4 ± 0.5 | 0.78 ± 0.55 | 2.1 ± 0.6 | −50 ± 22 |
| $L_3^*$ | Nov 2012 | 13.80 \| +0.38 | 38.68 \| +0.09 | 1.1 ± 0.5 | 1.04 ± 0.03 | 4.0 ± 1.1 | 4.0 ± 1.2 | 310 ± 20 | 7.2 ± 3.7 | −0.20 ± 0.10 | 6.6 ± 0.6 \| 6.7 ± 0.6 | 1.10 ± 0.52 | 3.6 ± 0.6 | −21 ± 28 |
| $L_4^*$ | Jul 2013 | 13.86 \| +0.51 | 38.70 \| +0.14 | 1.2 ± 0.5 | 1.06 ± 0.04 | 3.7 ± 1.7 | 8.2 ± 1.4 | 360 ± 10 | 3.3 ± 1.8 | −0.44 ± 0.23 | 5.5 ± 0.6 \| 5.1 ± 0.4 | 0.49 ± 0.44 | 1.7 ± 1.0 | −34 ± 61 |
| $L_1$ | Feb 2008 | 13.62 \| +0.36 | 38.65 \| +0.10 | 0.7 ± 0.5 | 1.01 ± 0.01 | 6.2 ± 1.5 | 8.4 ± 1.0 | 280 ± 80 | 5.4 ± 2.0 | −0.27 ± 0.10 | 5.8 ± 0.1 \| 6.6 ± 0.9 | 0.41 ± 0.19 | 2.4 ± 0.5 | −44 ± 26 |
| $L_2$ | Mar 2008 | 13.70 \| +0.37 | 38.65 \| +0.09 | – | – | – | – | – | – | – | – | – | – | – |
| $L_3$ | Nov 2009 | 13.57 \| +0.19 | 38.63 \| +0.05 | – | – | – | – | – | – | – | – | – | – | – |
| $L_4$ | Aug 2011 | 13.78 \| +0.32 | 38.66 \| +0.07 | 0.7 ± 0.5 | 1.01 ± 0.01 | 5.4 ± 0.8 | 15.9 ± 1.1 | 150 ± 50 | 2.5 ± 0.5 | −0.59 ± 0.12 | 5.5 ± 0.4 \| 5.7 ± 0.2 | 0.59 ± 0.13 | 1.3 ± 0.9 | −61 ± 30 |
| $L_5$ | Oct 2011 | 13.73 \| +0.31 | 38.66 \| +0.07 | 1.5 ± 0.5 | 1.13 ± 0.09 | 3.1 ± 1.7 | 5.2 ± 1.6 | – | 4.4 ± 3.0 | −0.33 ± 0.23 | 6.4 ± 0.2 \| 6.6 ± 0.1 | 1.44 ± 2.34 | 2.8 ± 1.0 | −38 ± 32 |
| $L_6$ | Nov 2011 | 13.73 \| +0.30 | 38.66 \| +0.09 | 0.8 ± 0.5 | 1.01 ± 0.01 | 5.4 ± 1.8 | 3.3 ± 1.0 | – | 12.0 ± 7.5 | −0.12 ± 0.08 | 6.4 ± 0.2 \| 6.2 ± 0.5 | 0.53 ± 0.27 | 3.6 ± 0.4 | −8 ± 24 |
| $L_7$ | Nov 2012 | 13.72 \| +0.28 | 38.66 \| +0.07 | 1.9 ± 0.5 | 1.17 ± 0.07 | 3.7 ± 1.1 | 5.7 ± 1.5 | 320 ± 10 | 4.7 ± 2.1 | −0.31 ± 0.14 | 6.1 ± 0.2 \| 6.2 ± 0.1 | 1.03 ± 0.80 | 2.6 ± 0.8 | −33 ± 23 |
| $G_1$ | Jan 2007 | 13.49 \| +0.21 | 38.60 \| +0.05 | 1.2 ± 0.5 | 1.02 ± 0.02 | 5.6 ± 2.0 | 5.2 ± 1.1 | 230 ± 30 | 7.9 ± 4.2 | −0.19 ± 0.10 | 5.8 ± 0.1 \| 5.5 ± 0.5 | 0.63 ± 0.36 | 2.6 ± 0.4 | −11 ± 10 |
| $G_2$ | Feb 2007 | 13.54 \| +0.33 | 38.61 \| +0.07 | 1.3 ± 0.5 | 1.03 ± 0.02 | 5.9 ± 2.1 | 8.2 ± 1.2 | 210 ± 10 | 5.2 ± 2.4 | −0.28 ± 0.13 | 5.3 ± 0.8 \| 5.2 ± 0.2 | 0.49 ± 0.31 | 2.0 ± 0.5 | −25 ± 25 |
| $G_3$ | Sep 2012 | 13.42 \| +0.21 | 38.59 \| +0.06 | 1.4 ± 0.5 | 1.02 ± 0.01 | 6.7 ± 1.3 | – | – | – | – | 5.9 ± 0.3 \| 5.1 ± 0.3 | 0.31 ± 0.12 | – | – |
| $G_4$ | Sep 2012 | 13.40 \| +0.19 | 38.59 \| +0.05 | 4.4 ± 0.5 | 1.33 ± 0.06 | 6.6 ± 1.5 | 7.5 ± 1.7 | 130 ± 30 | 6.5 ± 2.3 | −0.23 ± 0.08 | 5.0 ± 0.2 \| 5.2 ± 0.5 | 0.17 ± 0.09 | 1.8 ± 0.3 | −29 ± 23 |
| $G_5$ | Sep 2012 | 13.46 \| +0.23 | 38.60 \| +0.07 | 2.5 ± 0.5 | 1.07 ± 0.03 | 7.0 ± 2.0 | 8.6 ± 1.3 | 190 ± 90 | 5.9 ± 2.2 | −0.25 ± 0.10 | 5.4 ± 0.3 \| 5.6 ± 0.5 | 0.26 ± 0.13 | 2.0 ± 0.4 | −30 ± 26 |
| $G_6$ | Oct 2012 | 13.45 \| +0.18 | 38.60 \| +0.04 | 1.1 ± 0.5 | 1.02 ± 0.01 | 6.3 ± 1.5 | 5.1 ± 1.1 | 340 ± 70 | 9.0 ± 3.9 | −0.17 ± 0.07 | 5.2 ± 0.1 \| 5.4 ± 0.4 | 0.12 ± 0.08 | 2.1 ± 0.2 | −24 ± 20 |
| $G_7$ | Dec 2012 | 13.42 \| +0.20 | 38.60 \| +0.06 | – | – | – | – | – | – | – | – | – | – | – |

[a] $L_l^*$ refers to the LIW SCVs observed in the ligurian sea exhibiting the strongest $\theta/S$ signal, and $L_l$ (resp. $G_l$) to the others observed in the Ligurian Sea (resp. in the Gulf of Lions). $\theta$ (resp. $\Delta\theta$) is the absolute pot. temperature (resp. anomaly relative to the *far-field*) of the LIW observed within the SCVs core; $S$ and $\Delta S$ is the same for salinity; $d$ is the distance from the glider path to the SCVs center; $R$ is the SCVs radius defined as the distance between the two azimutal velocity extrema along the glider track; $\epsilon = \sqrt{1+d^2/R^2}$ is the scaling factor due to the glider sampling; $R_\epsilon = R \times \epsilon$ is the corrected radius; $V_\epsilon^{max} = |V^{max}| \times \epsilon$ is the corrected azimutal peak velocity; $P@V^{max}$ is the mean depth of the azimutal peak velocities; $T_r = 2\pi R/V^{max}$ is the rotation period; $Ro = 2V^{max}/fR$ is the Rossby number; $N_{scv}$ (resp. $N_{out}$) is the mean buoyancy frequency averaged around 400 m within the core of the SCVs (resp. in the *far-field* region); $Bu = [NH/fR]^2$ is the Burger number; $q_{scv}$ is the PV estimated within the core of the SCVs; $\delta q/q = (q_{scv} - q_{out})/q_{out}$ is the PV anomaly relative to the *far-field*. There are – where values could not have been computed due to a bad sampling.

signature in the surface layer of Atlantic Waters (AW) is found above them suggesting they are mostly isolated subsurface circulation features (see Figure 2b).

In the Ligurian Sea, less pronounced anomalies of the LIW characteristics were also identified with SCVs (hereafter referred as $L_i$, $i \in [1;7]$, see Table 1). They correspond to offshore LIW salinities comparable to those measured within the WCC (see Figure 3b). Further inspection on glider data in the Gulf of Lions also revealed the presence of SCVs characterized by a core of marked LIW (referred as $G_i$, $i \in [1;7]$). Their main properties are summarized in Table 1 along with the SCVs $L_i^*$ and they will further be discussed in section 3.2.5.

### 3.1.4. Location of Formation of the SCVs $L_i^*$

At the southwestern corner of Sardinia, the Sardinian Eddies are formed [*Testor et al.*, 2005a; *Testor and Gascard*, 2005]. They are very different in terms of characteristics and are associated with a propagation of LIW toward the southern basin. The southwestern corner of Sardinia is, to our knowledge, the northernmost bifurcation of the LIW flow toward either the southern basin, either northward along the continental slope. So, the preferential location of formation for the $L_i^*$, $L_i$, and $G_i$, which evolve in the northern basin, is probably situated downstream this point.

The strong positive $\theta/S$ anomaly of the SCVs $L_i^*$ indicates they most likely detach from the LIW vein flowing along the continental slope off Sardinia and Corsica, which transports LIW characterized by high $\theta/S$. The Figures 6a and 6b exhibits more closely how the LIW salinity evolves within this vein along its northward path. It has a more or less constant salinity along Sardinia (S $\sim$ 38.69), and then follows a general downstream decrease. At about the latitude of the Corsica-Sardinia strait (between 41°N and 41°N30′), a step-like decrease in the LIW salinity of about 0.02 can be observed, which suggests that important cross-shelf exchanges occur in this transition area. Noteworthy, the mean LIW salinity of $\sim$ 38.68 measured within the SCVs $L_i^*$ matches the mean observed salinity found at this transition, except for SCV $L_4^*$ that exhibits higher values. Due to dynamical barriers, SCVs are coherent and long-lived. The waters composing their cores are relatively protected from the ambient field and can present characteristics rather similar to those found at their formation area for long periods of time. We can therefore conclude that the SCVs $L_i^*$ were likely formed in the vicinity of the northwestern (NW) headland of Sardinia or upstream. Furthermore, Argo floats drifting velocities at $\sim$ 400 m depth along Sardinia and Corsica exhibit a transient drop at around 41°N30′ (see Figure 6c). The LIW flow seems hence to be less organized there likely revealing the presence of recirculation features consistent with a possible formation of SCVs there.

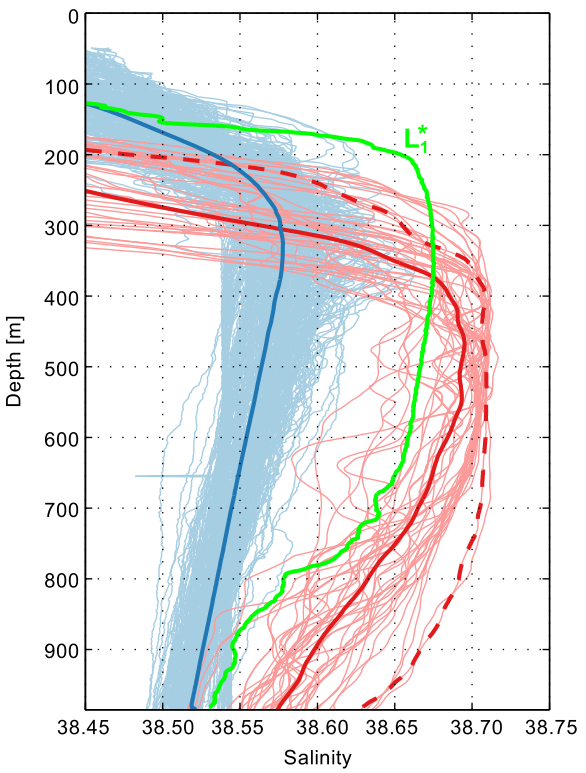


**Figure 5.** Salinity profiles collected along the "Nice-Calvi" glider section: within the offshore area (i.e., bottom depth > 2200m) (in blue), within the core of SCV $L_1^*$ (in green), and within the LIW vein flowing along Sardinia (39°30′N <lat. <41°10′N) (in red). The blue and red thick lines are the mean profiles, and the dashed red one represent the most homogeneous profile collected near the continental slope off Sardinia.

The SCV $L_4^*$ is clearly more saline than the others. That discrepancy in its core water properties can be interpreted as the result of the temporal variability of the LIW flow. Indeed, all the observations along the continental slope off Sardinia since 2013 (and a few in 2012) reveal greater salinity values than before (> 38.70), as revealed by the red dots in Figure 6b corresponding to the more recent observations. Noteworthy, the LIW salinity of the WCC also reaches its maximum value in June 2013 with about 38.68 (see Figure 3b). If this trend is confirmed in the future, it could lead to important changes in the cross-shelf heat/salt exchanges and the spreading of LIW toward the basin interior.

Concerning the SCVs $L_i$ and $G_i$, they present less marked characteristics and the method

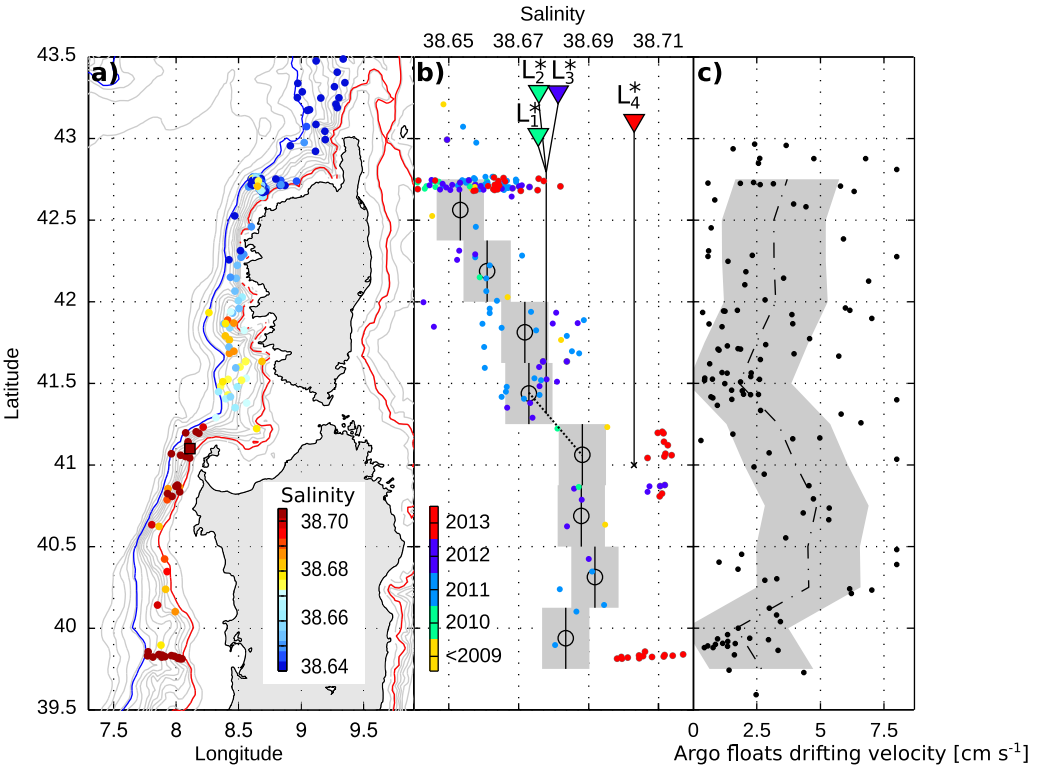


**Figure 6.** (a) LIW salinity observed by gliders, Argo floats, and shipborne CTD casts located between two *f*/*h* isolines (in red and blue defined by the 400 and 1800 m isobaths at 41°N). Isobaths are represented every 200 m. (b) LIW salinity against latitude: mean values were computed within 45 km intervals after having excluded outliers and values collected in 2013 (red dots). The gray-shaded area represent the standard deviation. The LIW values (triangles and vertical thin lines) found for each SCV $L_i^*$ are superimposed to show approximately their northernmost latitude of formation. (c) Argo floats drifting velocities at their parking depth (~ 400 m) against latitude (dashed line: mean value in 30 km intervals, gray shaded area: standard deviation).

of correspondence we used for the $L_i^*$, does not provide as useful information. According to this method, the area of possible locations of formation along the boundary circulation for $L_i$ or even more for $G_i$ is quite vast. It starts from the southern tip of Sardinia to the Gulf of Lions, where salinities $>$ 38.60 have been observed.

### 3.1.5. Propagation and Lifetime

The observations of the SCVs $L_i^*$ are separated of about 300 km along a straight line from their hypothetical formation zone. According to our advection estimates, the LIW SCVs appear to drift at about 2–5 cm s$^{-1}$, in agreement with previous studies [*Testor and Gascard*, 2003, 2006; *Pelland et al*., 2013]. They should then have spent 2–6 months to travel straight to their observation location. Although, the trajectories of SCVs are influenced by many processes:

1. The planetary $\beta$ effect: it drives the westward motion of eddies at a speed scaled by the phase speed of long Rossby waves [*Cushman-Roisin et al*., 1990]: in our case, given the small radius of the eddies the corresponding translation is not significant: $U_\beta \propto \beta R_d^2 \sim$ 0.05 cm s$^{-1}$ (with $\beta = 1.7\times10^{-11}$m$^{-1}$s$^{-1}$ and $R_d \sim 5$ km).
2. The topographic $\beta$ effect: as the LIW SCVs have a large vertical extend, they might have a small barotropic component, behave like Taylor columns and thus be influenced by the bottom topography. The typical scale for this translation given by the phase speed of long topographic Rossby waves: $U_{\beta_T} \propto \beta_T R_d^2 \sim$ 0.3–0.9 cm s$^{-1}$ (with $\beta_T = f\|\nabla h\|/h \sim 1-3\times10^{-10}$m$^{-1}$s$^{-1}$ and $R_d \sim 5$ km). This should not be very important too, except perhaps in the Gulf of Lions area where the topographic $\beta$ effect is the strongest of the basin away from the continental slope. It could favor the LIW SCVs to climb up the bottom slope of the Rhône Deep Sea Fan [*Carnevale et al*., 1991] and thereby reach the DWF zone in the Gulf of Lions, where they could then be trapped by the barotropic cyclonic circulation [*Madec et al*., 1996].
3. The effect of the barotropic mean flow (associated for instance with the NBF, planetary waves or mesoscale eddies): this was found to be a dominant process for the translation of coherent vortices [*Dewar*

*and Meng*, 1995], whereas baroclinic large-scale currents only have a weak influence on the propagation of nonlinear oceanic vortices due to the baroclinic $\beta$ effect [*Vandermeirsch et al.*, 2001].

4. Finally, all kind of interactions with dynamical structures (like eddies or jets) that the SCVs might encounter can also influence their translation.

Therefore, they should very likely have had much more complex paths across the basin and be characterized by much longer lifetimes. SCVs are known to be particularly long-lived circulation features. For instance, Meddies in the Atlantic [*Armi et al.*, 1988] or SCVs of newly formed deep waters in the Mediterranean Sea [*Testor and Gascard*, 2003, 2006] and in the Greenland Sea [*Gascard et al.*, 2002] can have a lifetime exceeding 1 year. Similarly, the LIW SCVs might also be able to live for a time order of a year or even more. During their slow decay, they could thus be able to spread out all over the NWMed.

### 3.2. Dynamical Properties and Diagnostics of the LIW SCVs

In order to better characterize these eddies, we calculate now some of their dynamical properties and buoyancy, heat, and salt content anomalies.

#### 3.2.1. Cyclostrophic Velocities

To estimate the velocity field within submesoscale anticyclones characterized by relatively strong horizontal shear ($> 0.1f$), one cannot only rely on the geostrophic balance. Indeed, nonlinear effects (i.e., the centrifugal force) need to be taken into account, otherwise the velocity would be underestimated [*Elliott and Sanford*, 1986].

The cross-section cyclostrophic velocities $v_c$ are therefore deduced by solving the quadratic equation expressing the gradient wind balance (and keeping the only relevant solution).

$$-v_c^2/r - fv_c = -fv_g \tag{2}$$

where $r$ the distance to the apparent eddy center, $f$ the Coriolis parameter, and $v_g$ the geostrophic velocities (method described in section 2.3). As for geostrophic velocities, the cyclostrophic velocities are also referenced thanks to the depth-average currents (minus the local mean advection, as explained in section 3.1.3) deduced by the gliders. In order to solve this equation, the last unknown remains the distance $r$ to the SCV center, which is not directly measured but can be estimated from the depth-average currents.

In a cylindrical coordinate system, the cyclostrophic velocities can be written as:

$$v_c(r) = \frac{rf}{2} \times \left(-1 + \sqrt{1 + 4Ro_g(r)}\right) \tag{3}$$

where $Ro_g(r) = v_g(r)/rf$ is the geostrophic Rossby number (constant for a quasisolid body rotation). In the present study, geostrophic Rossby numbers are about $-0.1$ to $-0.15$, so one can write: $v_c(r) \simeq v_g(r)\left\{1 - Ro_g(r) + 2Ro_g(r)^2 + \ldots\right\}$. $Ro_g(r)$ is negative for anticylonic eddies and thus cyclostrophic velocities exceed in magnitude the geostrophic ones. Small anticylones, characterized by a relatively high absolute Rossby number and for which the centrifugal force is not negligible, are then more energetic than what the only geostrophic balance would prescribe. For this reason, the cyclostrophic velocites are $\sim$10–15% greater than geostrophic velocities for the eddies considered in this paper.

#### 3.2.2. Eddy Center Detection

Following the approach of *Pelland et al.* [2013], we propose an objective method to geometrically determine the SCVs center position relative to the glider path thanks to the depth-average currents. For this purpose, we construct a cost function $g$ to minimize:

$$g(x,y) = \frac{1}{n}\sum_{i=1}^{n}\left(\mathbf{v_i} \cdot \frac{\mathbf{r_i}(x,y)}{\|\mathbf{r_i}(x,y)\|}\right)^2 \tag{4}$$

where $\mathbf{v_i}$ is the dive-average velocity estimated by the glider (minus the advection) at the given position $(x_i, y_i)$, and $\mathbf{r_i}(x,y)$ is the vector from $(x, y)$ to $(x_i, y_i)$. Minimizing this cost function finds the position in space which makes the depth-average currents the most perpendicular to the directions linking this position and the locations where the depth-average currents are measured. We applied this method to each SCV by taking at most four consecutive velocity estimates (minus the mean advection) centered around it in order to keep the measurements as synoptic as possible. This is equivalent to a temporal (spatial) interval of about

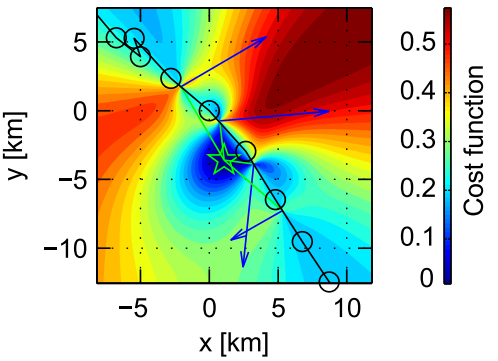


**Figure 7.** Depth-average currents (minus the mean advection) deduced by the glider while crossing SCV $L_2^*$. The cost function used to estimate the SCV center (green star) is shown by the colored contours.

$\sim$ 11 h ($\sim$ 11 km). Figure 7 illustrates the method by showing an example of the cost function minimization and the resulting eddy center estimation.

As the gliders did not cross the SCVs right at their center, we also estimated the scaling factor to apply to the apparent radius and velocities in order to compensate the underestimation of these parameters due to the glider sampling: $\epsilon=\sqrt{1+d^2/R^2}$ (Table 1) with $d$ the distance from the SCV center to the glider path and $R$ the apparent radius (defined as half the distance between the two azimutal velocity extrema). Note that $\epsilon$ is in general very close to unity. To compute the uncertainties shown in Table 1, we also considered a systematic error of 0.5 km on $d$, which corresponds to the SCVs being advected at $\sim$ 2.5 cm $s^{-1}$ in the cross-section direction during 11 h (the time window considered in the center detection method), which is a mean value considering all the different cases.

### 3.2.3. Rossby and Burger Numbers

The SCVs $L_i^*$ with the strongest $\theta/S$ signature have a radius and a velocity maximum of the same order of magnitude with a mean radius of 4.7 $\pm$ 1.0 km and a subsurface peak velocity of 6.6 $\pm$ 1.9 cm $s^{-1}$ located at intermediate depth within the LIW layer (see $L_i^*$ in Table 1). In case of quasisolid body rotation (Rankine vortex), the horizontal shear is constant within the core of the eddies and the Rossby number can be written as: $Ro=\zeta/f=(rf)^{-1}\partial_r(ru_r)=-2|V_{max}|/Rf$, with $\zeta$ the relative vorticity, $f$ the planetary vorticity, $|V_{max}|$ the azimutal peak velocity, and $R$ the eddy radius. The Rossby number of the SCVs $L_i^*$ is then on average $-0.29 \pm 0.11$. This value confirms that nonlinear terms are relatively important in the dynamical balance of the described SCVs, as previously hypothesized. Noteworthy, the Rossby number estimates should not vary with the distance $d$ (the glider path to the SCV center). In case of solid body rotation, the smaller apparent radius along the glider track will be indeed linearly compensated by a smaller observed velocity maximum: $Ro_\epsilon=-2\epsilon|V_{max}|/\epsilon Rf=Ro$. The radius corrected by the scaling factor ($R_\epsilon=\epsilon R$) is the order of the internal deformation radius or slightly smaller. It leads to high Burger numbers of 0.74 $\pm$ 0.27 ($Bu=[R_d/R]^2=[NH/fR]^2$ with $N$ ($=-g\partial_z\rho/\rho_0$) the buoyancy frequency in the *far-field* region at $\sim$400 m depth and $H$ defined as the water height where the salinity anomaly with the *far-field* profile exceeds 0.02). These values are within the stability bounds that were numerically computed for SCVs by *McWilliams* [1985]: $|Ro| \simeq 0.3 < Bu < 1$.

### 3.2.4. Potential Vorticity

Anticylonic SCVs are associated with a negative anomaly of the Ertel's Potential Vorticity (PV) field [*McWilliams*, 1985], which can be approximated in non-frontal areas by:

$$q=fN^2(1+Ro)/g \tag{5}$$

with $g$ the gravity and $N^2$ the squared buoyancy frequency.

We estimated the PV within each SCV by considering the measured stratification within their core ($N_{SCV}$) and their estimated Rossby number. Likewise, the PV of the surrounding waters ($q_{out}$) was computed with the estimation of $N_{out}$ and by assuming $Ro \ll 1$. $N_{SCV}$ and $N_{out}$ are considered as the mean value of $N$ between 450 and 550 m depth. The negative PV anomalies associated with each SCV relative to the *far-field* region are then of about $-39\% \pm 14$ (see Table 1), in agreement with the values found by *Pelland et al.* [2013] for dynamically similar anticyclonic SCVs.

The Ertel's PV of an isolated fluid parcel is conserved in absence of nonconservative processes. The logarithmic form of the PV conservation allows to better assess the contribution of the different terms in equation (5):

$$\frac{\Delta q}{q}=\frac{\Delta f}{f}+\frac{\Delta Ro}{1+Ro}+\frac{\Delta N^2}{N^2}=0 \tag{6}$$

The PV of the SCVs $L_i^*$ presented in Table 1 should have been well conserved since their formation, since they exhibit a strong $\theta/S$ signature and mixing should not have been acting much on them. In the

following, we discuss the PV balance of a typical SCV from its formation (at the NW corner of Sardinia) to its observation (at 43°N with a Rossby number of −0.3):

1. The first term of the balance ($\Delta f/f$) is negligible since the SCV has drifted to the north about 2° in latitude, which implies $\Delta f/f = 0.04 \ll 1$.
2. Assuming the SCV to be formed from the LIW vein flowing along Sardinia, whose initial Rossby number should remain small at the scale of the vein ($Ro \simeq -0.05$, considering a horizontal shear of 5 cm $s^{-1}$ decreasing over 10 km), it yields: $\Delta Ro/(1+Ro) = -0.26$.
3. In the end, one can estimate the stratification of the boundary flow from which the SCV has been formed. Considering the SCV to have a core stratification of 6.0 $f$ (see Table 1), we then found $N_{init} = 7.0f$.

Inspecting the density profiles collected within the LIW vein along Corsica and Sardinia (between the red and blue $f/h$ isolines shown in Figure 6a), we found a stratification of 6.1 ± 0.6 $f$ north of 42°N, and a slightly greater stratification of 6.9 ± 0.6$f$ south of 41°15′. This latter value is in good agreement with $N_{init}$ previously estimated, which gives an additional dynamical argument to support the idea of a flow detachment occurring at the latitude of the northwestern corner of Sardinia.

#### 3.2.5. Case of the LIW SCVs $L_i$ and $G_i$

Since 2007, other glider deployments in the Gulf of Lions and in the Ligurian Sea also revealed the presence of LIW SCVs (their observation location is shown by diamond in Figure 1, see also Figure 8 for a typical example). Their absolute LIW $\theta/S$ characteristics are less pronounced ($\theta < 13.8$°C and $S < 38.68$). Noteworthy, the SCVs $G_i$ were observed in the vicinity of the Deep Water Formation (DWF) zone of the Gulf of Lions where the background LIW salinity is low (see Figure 1). The mean LIW $\theta/S$ anomalies of the SCVs $L_i$ and $G_i$ present a greater range but remain significant compared to the *far-field* (+ 0.26 ± 0.07°C and + 0.07 ± 0.02).

In order to assess their key dynamical characteristics, we applied to the SCVs $L_i$ and $G_i$ the same methodology as previously described (see Table 1 for an exhaustive list of their characteristics). They are dynamically characterized by:

1. slightly greater radii (5.9 ±0.9 km) and peak azimuthal velocities of same order of magnitude (6.4 ±1.9 cm $s^{-1}$, without considering the very energetic SCV $L_4$, see Table 1) compared to, respectively, 4.7 ± 1.0 km and 6.6 ± 1.9 cm $s^{-1}$ for the SCVs $L_i^*$;
2. slightly smaller Rossby numbers of −0.24 ± 0.07 (except the very non-linear SCV $L_4$, see Table 1) compared to 0.29 ± 0.11;
3. slightly smaller Burger numbers of about 0.45 ± 0.27 compared to 0.74 ± 0.27.

## 4. Discussion

### 4.1. Formation Processes of the LIW SCVs $L_i^*$ at the NW Headland of Sardinia

Arguments based on hydrography, the drift of Argo floats and the PV conservation previously exposed in section 3.1.4 support the idea that the SCVs $L_i^*$ likely originate from the northwestern part of Sardinia. In this section, we further discuss the potential formation mechanisms of these particular LIW SCVs. We also highlight the important role of the complex topography and of the water masses circulation off western Sardinia for their generation.

#### 4.1.1. Generation Mechanisms of LIW SCVs

A generation mechanism of anticyclonic SCVs was first described by *McWilliams* [1985]:

1. a phase of vertical diapycnal mixing that lowers the PV of a fluid parcel;
2. a phase of intrusion into a more stratified environment;
3. a phase of cyclostrophic adjustment that isolates the fluid parcel of low PV within the core of an anticyclonic SCV.

In our case, the PV reduction cannot be caused by winter vertical mixing due to air-sea interactions, since the SCVs are made of remote intermediate waters disconnected from the air/sea interface. In addition, they

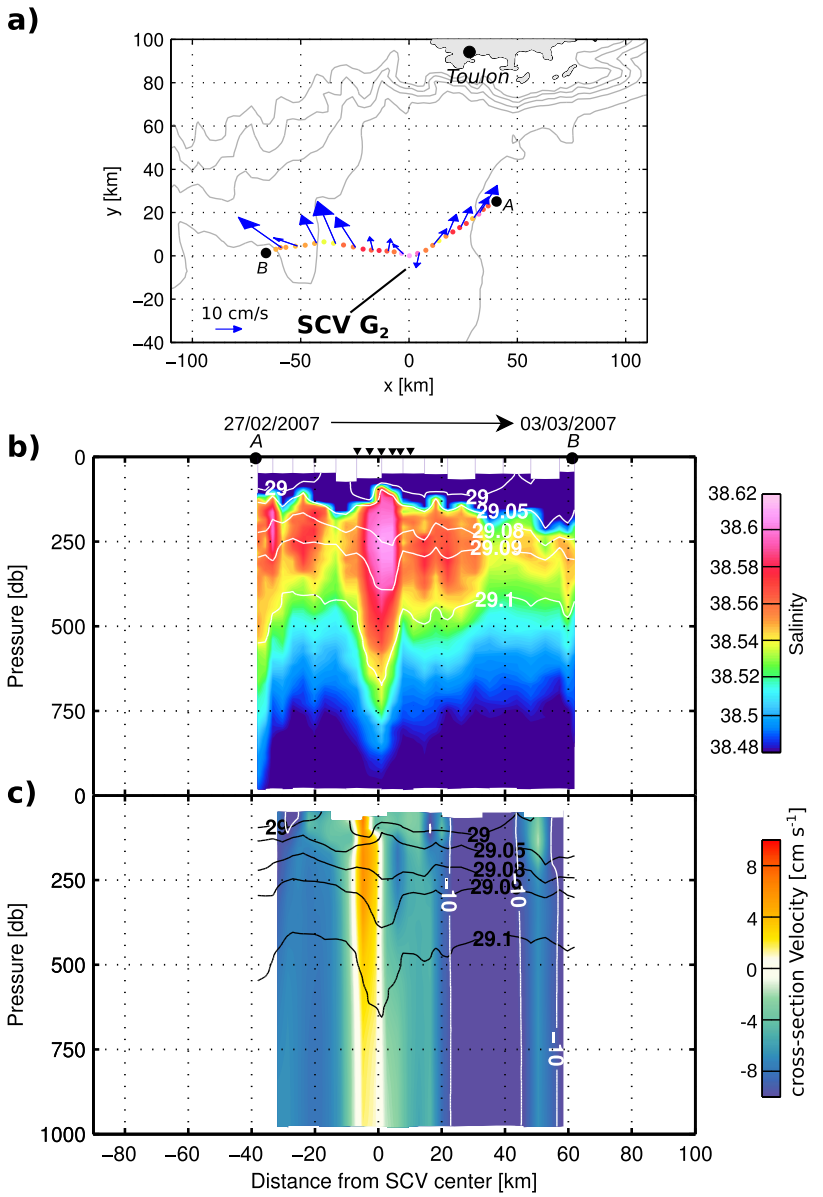


**Figure 8.** Glider deployment in the Gulf of Lions in February 2007 revealing the presence of SCV $G_2$: (a) Glider pathway with the LIW salinity of each profile colored according to the colorbar of (b) and depth-average currents deduced by the glider minus the mean advection. (b) Salinity section with density contours in white. Black triangles show the position of glider profiles carried out within the SCV. (c) Cross-section cyclostrophic velocities with contours in cm $s^{-1}$. The black contours show the smoothed density field used to integrate the thermal wind balance.

are so pronounced in $\theta/S$ that they cannot result from the mixing of LIW with the fresh surface layer of Atlantic Waters (AW).

The interaction of a current with a sloping boundary was then identified as another potential PV sink [*D'Asaro*, 1988]. Nonconservative frictional effects, which can drive diapycnal mixing as well as the creation of anticyclonic vorticity within the bottom boundary layer (BBL), act at reducing the PV. Progressively a patch of low PV can thereby be formed, leading to the formation of SCVs, if the flow is eventually able to detach from its boundary [*D'Asaro*, 1988].

Evidence of mixing is found close to the continental slope along NW Sardinia, where salinity profiles collected there exhibit a relatively homogeneous layer of LIW compared to ordinary profiles having a sharper salinity maximum (see red profiles compared to blue ones in Figure 5). Furthermore, the Figure 5 shows strong similarities between the most homogeneous salinity profile collected off Sardinia and the salinity

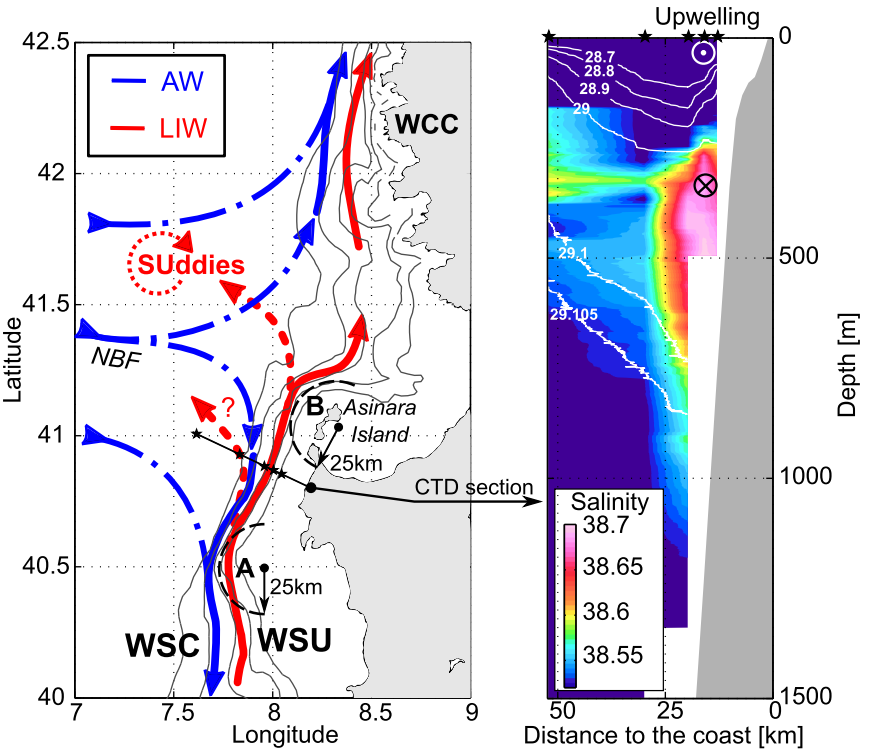


**Figure 9.** (left) Main circulation pathways of the AW (in blue) and of the LIW (in red) in the vicinity of the NW headland of Sardinia (isobaths are drawn every 500 m). The flows associated with the Western Corsica Current (WCC), the North-Balearic Front (NBF), the Western Sardinian Current (WSC), and the Western Sardinian Undercurrent (WSU) are shown. The two locations suitable for a flow detachment that can lead to the formation of the Suddies are also labeled by capital letters A and B. (right) A salinity section off NW Sardinia from CTD casts carried out in April 2013.

profile collected within the core of a typical LIW SCV. Strong negative vorticity ($\sim -f$) could directly come from the BBL presenting a strong horizontal shear, even if the currents might not exceed 5 cm $s^{-1}$ at intermediate depths, as stated by *Pelland et al.* [2013]. Besides, the continental slope becomes steeper north of 40°N30′ off western Sardinia (dowstream point A in Figure 9). If the BBL thickness remains approximately constant along the LIW flow, the horizontal shear will likely be enhanced there (i.e., stronger negative vorticity). If this horizontal shear, then becomes so negative that $\zeta < -f$, the fluid can undergo ageostrophic centrifugal instability. This was recently revealed by the model study of *Molemaker et al.* [2014], which highlights the importance of the centrifugal instability as a source of turbulent mixing for the generation of subsurface eddies from the California Undercurrent. At last, additional sources of diapycnal mixing within the LIW vein could come from the adjustment of the geostrophic flow over the continental slope [*Benthuysen and Thomas*, 2012], and/or the turbulence generated by near-inertial internal waves, which can also be a great source of mixing over the continental slope even at great depths [*van Haren et al.*, 2013].

### 4.1.2. Flow Detachment at the NW Headland of Sardinia

Observations [*Noble and Ramp*, 2000] and theoretical considerations [*Allen*, 2000] have shown that steady flow cannot remain parallel to isobaths when they converge relatively quickly in space, as it is the case near the point A in Figure 9. These converging isobaths cause an inherent change in the continental slope (isobaths 500 and 2500 m are separated from about 50 km upstream of A and then only from about 20 km downstream). The spatial acceleration forces, which result from the focusing of a broad, slow flow over gently sloping topography into a faster, narrower current over steeper topography, can override vorticity constraints. The current cannot then turn rapidly enough to follow the topography. The complex topographic constraints observed at the NW part of the Sardinian continental slope could thus be a preferential site for generating undercurrent meanders.

Concerning the flow detachment, *Marshall and Tansley* [2001] have found a criterion for a current flowing along a wall: $r < (U/\beta)^{1/2} \simeq 55$ km, where $U \sim 5$ cm $s^{-1}$ is the typical speed of the current (measured by the

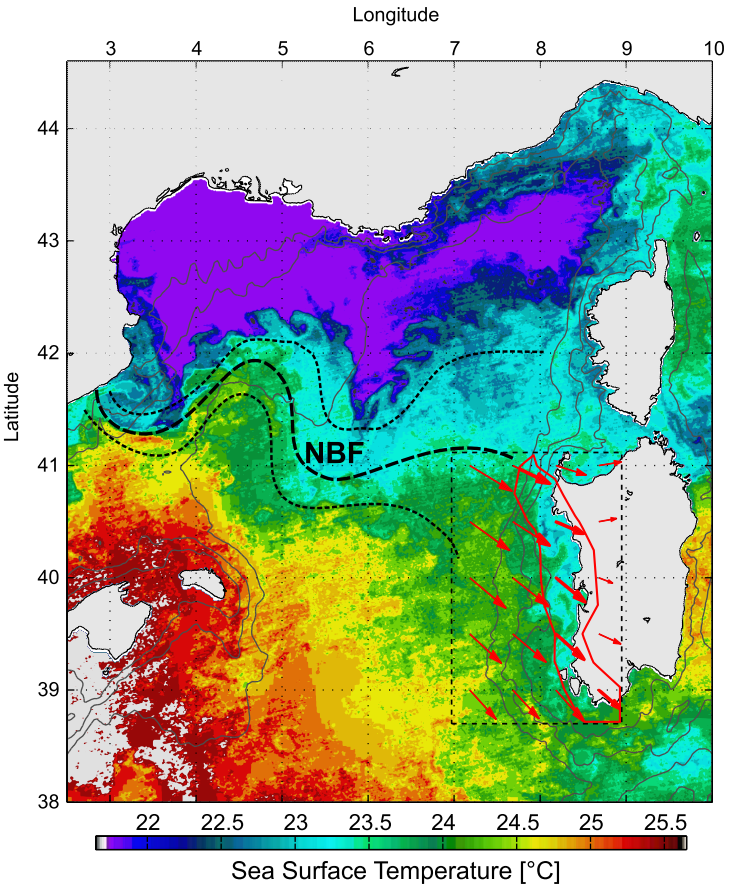


**Figure 10.** SST observed by satellite on the 26 September 2012 during an upwelling situation along the Sardinian coast. The ECMWF mean wind field (2007–2011 period) is superimposed and the red contours highlight the area of positive Ekman pumping along the western coast of Sardinia. The North Balearic Front (NBF) can also be identified by the 24°C isotherm. Isobaths at 500, 1500, and 2500 m are also depicted.

drift of Argo floats shown in Figure 6c), $r$ the curvature of the wall and $\beta = 1.7 \times 10^{-11} m^{-1} s^{-1}$ the planetary vorticity gradient in the downstream direction. In the vicinity of the NW headland of Sardinia, the curvature associated with two eastward veerings of the topography is much smaller ($\sim$ 25 km) than this critical value as shown by the circles representing the curvature of the continental slope around the two locations labeled by A and B in the left plot of Figure 9. It thus supports a potential shedding of the SCVs by flow detachment at the NW part of the Sardinian continental slope. The similar process of flow detachment was previously pointed out for the formation of the larger SEs at the southwestern corner of Sardinia [*Testor et al.*, 2005a].

#### 4.1.3. Mean Circulation Along the Western Coast of Sardinia

Surface drifters trajectories [*Poulain et al.*, 2012] and numerical studies [*Olita et al.*, 2013; *Pinardi et al.*, 2013] identified a stable southward surface flow along the western continental slope of Sardinia. Furthermore, SST images often exhibit a cross-shore positive temperature gradient, corresponding to upwelling situations associated with this southward surface current. As a matter of fact, the western coast of Sardinia is an area of mean wind direction favorable to upwelling (northwesterlies) and positive Ekman pumping (see Figure 10). On the contrary to the upwelling along the southern coast of Sicily [*Piccioni et al.*, 1988], this upwelling system has not been much studied so far. The only recent numerical study by *Olita et al.* [2013] identified the combined action of winds and anticylonic eddies (like SEs or AEs) as potential drivers of this southward current, named the Western Sardinian Current (WSC) in this study. It can also be considered as a surface branching of the eastward flow associated with the NBF: a part could flow toward the Algerian basin along the Sardinian coastline, while another part would flow northward along Corsica and form the WCC as shown by Figure 9 (left).

The Figure 9 (right) represents a CTD section carried out off the NW headland of Sardinia in April 2013. A southward surface current associated with an uplift of the isopycnals over 0–200 m is prevailing showing that the LIW flow can be a northward undercurrent flowing close to the continental slope (width of the vein $\simeq$ 10 km) and being thus somehow isolated from the southward surface flow of AW. We will further refer to this circulation feature as the Western Sardinian Undercurrent (WSU) (see Figure 9). For the WSU, typical velocities of $\sim$ 5 cm $s^{-1}$ at about 400 m depth can be inferred from the drift of Argo floats around 41°N (see Figure 6c). Note that the presence and the variability of this current system making the LIW vein appear as an undercurrent is not currently well known. This is likely not a permanent situation but can at least occur on a transient basis.

In the WCC and further downstream in the NC (see Figure 1), AW and LIW flow in the same direction. The current has a barotropic-equivalent structure with surface intensified velocities [*Millot*, 1999]. This can clearly

be seen in the Nice-Calvi velocity section shown in Figure 2c. If an eddy is then formed from such a barotropic-equivalent boundary current (by baroclinic instability for instance), this latter would likely keep its surface-intensified structure (like for the AEs) [*Millot et al*., 1990] with a surface core made up of fresher AW compared to the more modified AW found offshore. However, the SCVs we observed have no significant surface velocities due to the deformation of isopycnals associated with their cores that implies a decrease of the velocities toward the surface, as well as no core of fresher AW (see Figure 2b). The presence of a southward surface current at the NW part of Sardinia seems therefore to be an important condition for their formation.

As the WSU seems to be at the origin of the SCVs similar to the SCVs $L_i^*$, we propose to name them "Suddies," standing for "Sardinian Undercurrent eddies."

### 4.2. Origin of the SCVs $G_i$ and $L_i$

All the LIW SCVs ($L_i^*$, $L_i$, and $G_i$) present strong dynamical similarities (see Table 1) and since we know the Suddies ($L_i^*$) would be able to reach the Gulf of Lions area due to their extended lifetime ($\sim$ 1 year) and to their typical translation of a few kilometers per day, one could argue $L_i$ and $G_i$ could very well be of the same origin and be less marked owing to the fact that these SCVs decayed. The stage at which a SCV is observed is actually an unknown to take into account: as a SCV gets older, it would present less marked properties being though still marked compared to the ambient waters. So, since the characteristics of the LIW in the boundary current decrease along its path, the comparison between the core characteristics of a LIW SCV and the LIW characteristics in the boundary circulation, gets a less accurate tool for determining the location of formation of such a SCV. Both its age and the properties of its core determine the downstream and upstream limits of the area of possible locations of formation. As a matter of fact, the observations of the four very well-marked $L_i^*$ in the Ligurian Sea imply they were relatively young eddies and the area of possible locations of formation is relatively small: it encompasses the boundary circulation between the northeastern tip of Sardinia and the southwestern corner of Sardinia. For $L_i$ and $G_i$, this is less clear since they contain less pronounced LIW that has mixed with surrounding waters.

We have no undeniable arguments $L_i$ and $G_i$ are really old Suddies that have traveled from a location of formation located around the northwestern tip of Sardinia. As far as the hydrography is concerned, they could be formed much further downstream. Depending on the LIW SCV, it could concern vast areas such as the whole boundary circulation from the southwestern corner of Sardinia to the Gulf of Lions. However, *McWilliams* [1985] stated baroclinic or barotropic current instabilities might not be able to generate isolated anticyclonic SCVs and their extreme low PV core. Diapycnal mixing [*McWilliams*, 1988] and the interaction with sharp topography [*D'Asaro*, 1988] should be the two main sources for the generation of SCVs. As previously argued in section 4.1, only the second mechanism can be retained for the generation of SCVs carrying LIW, the first one being dedicated to the formation of mode waters SCVs formed by winter vertical mixing [*Gascard et al*., 2002; *Testor and Gascard*, 2003]. There are two important points to highlight, if one tries to guess preferential locations of formation of such eddies:

1. the potential role of the topography, associated with both the curvature effects and with the vertical mixing of the LIW vein.
2. the potential role of the doming of the isopycnals separating the LIW vein from the AW above in the boundary circulation.

Concerning the first aspect, a site-like south of Toulon could very well be another preferential site for the generation of SCVs because of the curvature of the slope there. Concerning the second aspect, to our knowledge, the northwestern part of Sardinia is the only place in the boundary circulation of the western Mediterranean sea where this has been observed. For periods of time, it can be characterized by a system composed of a surface flow flowing southward on the opposite of the LIW flowing below, according to the general cyclonic circulation of the basin. Elsewhere, the boundary circulation in this basin is known to be barotropic-equivalent with all the water masses flowing in the same direction [*Millot*, 1999]. This could be a crucial aspect for the formation of such SCVs, and if so, $L_i^*$, $L_i$, and $G_i$ would then likely originate from the same location.

Furthermore, we found since 2007 about 50 shipborne CTD casts and Argo floats profiles revealing significant salinity anomalies relative to the climatological LIW salinity field. They are characterized by anomalies that are

twice greater than the standard deviation of the observations minus the objectively analyzed LIW salinity field that was presented in section 2.2 (see black circles in Figure 1). These isolated profiles clearly demonstrate the presence of well-marked LIW offshore but are not clear evidences of the presence of LIW SCVs. They are individual profiles with no information on their vicinity. Moreover, the sampling strategy of the Argo profiling floats in the NWMed is about 4–5 days between two surfacings. At this sampling frequency, the anticyclonic rotation period of 6.1 ± 2.4 days associated with those LIW SCVs is then too much aliased. These profiles could only be considered as the potential signatures of LIW SCVs. Nevertheless, the high concentration of such salinity anomalies in the vicinity of the NW headland of Sardinia reinforces the idea of a privileged site for lateral heat/salt exchange at intermediate depth likely related to the formation of the Suddies.

### 4.3. Implication of LIW SCVs on Mixing Processes in the NWMed

In this section, we first try to infer a production rate of LIW SCVs at the NW headland of Sardinia, which is thought to be likely a preferential generation site for LIW SCVs. By doing so, we aim to estimate the impact of such dynamical structures on the basin-scale spreading of the LIW and to discuss their implications for the deep water formation. In particular, due to their high heat and salt content and to their perturbation of the ambient stratification, they could locally help the deepening of the mixed layer.

#### 4.3.1. Production Rate of LIW SCVs and Impact on the Basin-Scale

We can estimate a production rate of Suddies at the NW corner of Sardinia from the LIW salinity decrease of about $\Delta S_c \sim 0.02$ observed within the boundary flow between 41°N and 41°N30′ (see Figure 6b). This would imply a net salt flux toward the open sea: $\Phi_c = UR_c h_c \Delta S_c$, with $U$ the mean current of the LIW flow, $R_c$ its approximate width, and $h_c$ its thickness. In doing so, we assume that the transport of the LIW flow (defined as $UR_c h_c$) is constant between the two considered latitudes. Finally, dividing $\Phi_c$ by the positive salt anomaly available in one single SCV: $\Phi_e = \pi R_e^2 h_e \Delta S_e$ (with $R_e$ the radius of the SCV, $h_e$ its height and $\Delta S_e$ its typical salinity anomaly), we end up with a production rate of:

$$\frac{\Phi_c}{\Phi_e} = \frac{\alpha U R_c \Delta S_c}{\pi R_e^2 \Delta S_e} \tag{7}$$

where $\alpha = h_c/h_e = (1+Ro_e)/(1+Ro_c)$ (deduced from the PV conservation, PV $\propto (1 + Ro)/h$). One can then assume $U \sim 3$–$5$ cm s$^{-1}$ (from Argo floats drifting velocities, see Figure 6c) and $R_c = 10$ km (from the CTD section, see Figure 9), which implies a Rossby number of the LIW flow $Ro_c = -(0.03$–$0.07)$. As the SCVs signature is not only restricted to their dynamical core, we consider $R_e \sim 7$ km which is slightly greater than the mean radius reported in Table 1. Considering $\Delta S \sim 0.1$ and $Ro_e \sim -0.3$ ($\Rightarrow \alpha = 0.72$–$0.75$), it yields a production rate of about 10–15 SCVs per year. We should although consider a smaller proportion from this range as some terms of the salt balance have been neglected (the vertical mixing or the upwelling effect, for instance) and other cross-shelf exchanges might be at play.

In addition, we observed 4–10 LIW SCVs (the 4 $L_i^*$ + the 6 $L_i$, if we assumed $L_i$ are old Suddies) along the Nice-Calvi section in 4 years (1–2.5 SCVs per year observed on average), but we might have missed lots of them. The open ocean portion of the Nice-Calvi section was only occupied by glider missions about 20% of the time from July 2009 to July 2013. Statistically, we could therefore have observed up to 5–12.5 SCVs per year in the only Ligurian Sea. On this basis, we can therefore hypothesize they are in total order of 10–20 to be formed each year, which is slightly more than the number estimated before. Note that this latter estimate is the same order as the first one related to a formation site at the NW corner of Sardinia. So, there might be a few places where SCVs are formed in parallel to the formation of Suddies at the NW headland of Sardinia, but not that many.

The formation of 20 SCVs per year at the only NW corner of Sardinia may, however, be unrealistic because that would imply an eddy formed every 18 days, which is too close from the ∼ 6 days rotation period of those eddies. The order of magnitude for the number of Suddies formed each year should thus be around 10 (± 5), a greater precision on this number can hardly be achieved from the present data set.

Whatever their origin, the LIW SCVs are observed all over the whole NWMed from the Ligurian Sea ($L_i^* + L_i$) to the Gulf of Lions ($G_i$) and present heat/salt content anomalies of about the same order (see Table 2 and Appendix A). The mean heat (resp. salt) content anomaly transported by LIW SCVs can be estimated to about $(8.5 \pm 5.7) \times 10^{16}$ J (resp. $(5.7 \pm 3.4) \times 10^9$ kg). So, their impact could be quantified at the basin scale independently of their location of observation. Given the extended lifetime of SCVs, their complex

**Table 2.** Heat/Salt Content Anomaly[a]

| | $L_1^*$ | $L_2^*$ | $L_3^*$ | $L_4^*$ | | | |
|---|---|---|---|---|---|---|---|
| Lat./Lon. | 43°00′N/8°25′E | 43°18′N/8°00′E | 43°23′N/8°55′E | 43°05′N/8°14′E | | | |
| $\Delta HC$ ($\times 10^{16}$ J) | 11.5 ± 3.2 | 4.3 ± 5.9 | 4.9 ± 1.4 | 5.4 ± 2.4 | | | |
| $\Delta SC$ ($\times 10^{9}$ kg) | 7.7 ± 2.2 | 9.2 ± 3.8 | 2.1 ± 0.6 | 2.2 ± 0.9 | | | |
| | $L_1$ | $L_2$ | $L_3$ | $L_4$ | $L_5$ | $L_6$ | $L_7$ |
| Lat./Lon. | 42°23′N/7°34′E | 43°26′N/7°44′E | 43°23′N/7°55′E | 43°07′N/8°14′E | 43°21′N/7°55′E | 43°09′N/8°13′E | −43°03′N/8°18′E |
| $\Delta HC$ ($\times 10^{16}$ J) | 7.4 ± 1.9 | – | – | 24.4 ± 3.5 | 8.5 ± 4.7 | 2.6 ± 0.9 | 6.3 ± 1.9 |
| $\Delta SC$ ($\times 10^{9}$ kg) | 6.3 ± 1.6 | – | – | 12.7 ± 2.0 | 3.6 ± 2.0 | 3.2 ± 1.1 | 3.3 ± 1.1 |
| | $G_1$ | $G_2$ | $G_3$ | $G_4$ | $G_5$ | $G_6$ | $G_7$ |
| Lat./Lon. | 42°19′N/5°36′E | 42°17′N/5°34′E | 42°05′N/4°20′E | 42°00′N/5°00′E | 42°04′N/4°34′E | 42°00′N/4°39′E | 41°49′N/4°37′E |
| $\Delta HC$ ($\times 10^{16}$ J) | 8.2 ± 2.8 | 8.0 ± 2.8 | 17.5 ± 3.5 | 6.8 ± 1.7 | 11.8 ± 3.3 | 3.0 ± 0.8 | 5.6 ± 3.6 |
| $\Delta SC$ ($\times 10^{9}$ kg) | 4.6 ± 1.6 | 4.8 ± 1.7 | 8.1 ± 1.7 | 6.9 ± 1.8 | 11.2 ± 3.3 | 1.5 ± 0.4 | 4.5 ± 2.9 |

[a]Lat. (resp. Lon.) is the latitude (resp. longitude) where each SCV was observed. $\Delta HC$ (resp. $\Delta SC$) represents their integrated heat (resp. salt) anomaly relative to the *far-field*.

translation and the observation of similar but the less marked SCVs in the Gulf of Lions, one can make the basic assumption that LIW SCVs are present more or less uniformly over the NWMed.

To get an order of magnitude of the effect of LIW SCVs at the basin scale, lets consider a yearly production and dissipation of 10 ± 5 LIW SCVs (about the production rate of the Suddies at the NW corner of Sardinia, or about the production rate LIW SCVs more generally, that were estimated above). It would then result in a heat/salt input spread out over the whole basin surface of about $(1.1 \pm 1.0)\times 10^{18}$ J yr$^{-1}$ and $(7.5 \pm 6.2)\times 10^{10}$ kg yr$^{-1}$. The offshore part of the basin-scale cyclonic gyre (delimited by the black arrows in Figure 1) having a surface of about $150\times 10^{3}$ km$^2$, the resulting heat/salt input is then equivalent to, respectively, $\Phi_\theta = (7.3 \pm 6.7)\times 10^{6}$ J m$^{-2}$ yr$^{-1}$ ($\Longleftrightarrow$ 0.23 ± 0.21 W m$^{-2}$) and $\Phi_S = (0.50 \pm 0.41)$ kg m$^{-2}$ yr$^{-1}$. Assuming a LIW layer thickness of 500 m, this heat/salt input at mid depths will then contribute to the heating (+0.0036°C yr$^{-1}$) and salting (+0.0010 yr$^{-1}$) of the LIW of the NWMed.

#### 4.3.2. Implications for the WMDW Properties and the Western Mediterranean Transient

The DWF zone represents about 10% of the total surface of the NWMed (see location in map of Figure 1). *Durrieu de Madron et al*. [2013] estimated it to 15 × 10$^3$ km$^2$ from ocean color images during the deep convection event of winter 2012, which is known as a strong convective event. So, assuming the random presence of 10 ± 5 LIW SCVs over the whole basin (lifetime order of 1 year), there could be 1 or 2 LIW SCVs located within the DWF zone prior to deep mixing events. The vertical mixing in winter would then directly transfer the excess of heat and salt associated with such SCVs into the mixed patch warming and salting the newly formed deep waters. This positive heat (resp. salt) anomaly contained in 1–2 typical LIW SCVs distributed over the whole volume of the DWF zone (mean depth ∼2000m) would then be equivalent to an increase of +0.0012 ± 0.0009°C (resp. +0.00031 ± 0.00027) of the newly formed WMDW characteristics compared to the water mass that would have been formed in the absence of such warm and salty LIW SCVs. The only presence of a few LIW SCVs within the DWF zone at the onset of the convection could then still be significant enough to have a measurable impact on the $\theta/S$ properties of the newly formed deep waters. Moreover, if the lifetime of LIW SCVs exceeds the 1 year hypothesized, this would increase proportionally the contribution of the LIW SCVs to the WMDW characteristics.

*Bethoux et al*. [1990] reported a constant warming (0.004°C yr$^{-1}$) and a subsequent salting (density compensated) of the WMDW from the 1960s to the 1990s. The only impact of the LIW SCVs on the WMDW properties could thus explain 8–53% of this trend. Therefore, they seem to be major vectors of heat and salt transfer down to the deep ocean of the western Mediterranean Sea.

In 2005, a major production of anomalously warm and salty deep waters occurred in the Gulf of Lions [*Schroeder et al*., 2006]. This event was named the Western Mediterranean Transient (WMT) since *Schroeder et al*. [2010] suggested it was the consequence of the westward propagation of the Eastern Mediterranean Transient (EMT). The EMT is a shift in the deep water formation site of the eastern Mediterranean Sea [*Malanotte-Rizzoli et al*., 1999] that led to an increase in the heat/salt injected at the Sicily channel into the western Mediterranean Sea [*Gasparini et al*., 2005]. The direct implication of the EMT being still in debate, observations [*Schroeder et al*., 2010] and a numerical study [*Herrmann et al*., 2010]; however, both agree on the fact that this particular deep convection event was likely triggered by an accumulation of heat and salt

at intermediate depths. This heat and salt accumulation could then have been transferred to great depths by deep vertical mixing, thus drastically affecting the properties of WMDW ($+0.038^{\circ}$ and $+0.0012$ reported by *Schroeder et al*. [2008]). While *Schroeder et al*. [2010] attributed a major role to the lateral heat/salt advection, *Herrmann et al*. [2010] gave more importance to the weakness of the winter buoyancy loss in the NWMed that prevented strong convection to occur during the 1990s, enabling the heat and salt content of the intermediate layers to regularly increase in this region.

The estimated fluxes due to the LIW SCVs, $\Phi_\theta \sim +0.7\times10^7$ J m$^{-2}$ yr$^{-1}$ and $\Phi_S \sim +0.5$ kg m$^{-2}$ yr$^{-1}$ remain two order of magnitude smaller than the lateral heat/salt flux estimated by *Schroeder et al*. [2010]. In a classical framework, where deep convection occurs regularly, they cannot alone explain this brutal transition. Nonetheless, if there were no significant deep convection events during a long period prior to the convective event of 2005 (as being thought during the 1990s), the heat and salt flux toward the basin due to the LIW SCVs could have significantly increased the heat and salt content of the intermediate layers of the basin. This heat and salt accumulation leading to more marked LIW in the NWMed could then have been transferred into the deep by the exceptionally strong convection event of winter 2005. One would have to consider the heat/salt transported by about 10 LIW SCVs formed and dissipated every year, integrated over 5–10 years, plus the contribution of the LIW SCVs directly implicated in the DWF to explain about 13–25% of the changes in the WMDW properties observed in 2005.

Overall, these numbers provide only orders of magnitude but they would indicate that the LIW SCVs, being numerous and able to transport well-marked LIW into the deep convection area, can have a significant role in setting up the WMDW characteristics, among the other processes at play (LIW advection by other means, AW characteristics, atmospheric forcing).

#### 4.3.3. Winter Mixing Preconditioning

The presence of LIW SCVs in an area of strong winter buoyancy loss like the Gulf of Lions or the Ligurian Sea can act as a local preconditioning agent of the winter mixing (see Figure B1 in Appendix B). They could hence substantially impact the spatial distribution of the mixed layer, when winter mixing starts to be at play. For instance, assuming a LIW SCV similar to $L_2^*$ being subjected to a cumulative buoyancy loss of 0.4 m$^2$ s$^{-2}$ (about the buoyancy loss of five winter storms, see numbers presented in Appendix B), the mixed layer will then vary from $\sim$ 500m outside the SCV to more than 1000 m in its core (see Figure B1). They would therefore induce very localized, but important modulations of the mixed layer depth. The effect of localized convection at the mesoscale was first suggested by *Gascard* [1978] in the NWMed and then numerically studied by *Legg et al*. [1998]. Similar effects of the local preconditioning by SCVs remnants of the previous winter were also revealed in the Greenland Sea [*Lherminier et al*., 1999; *Gascard et al*., 2002]. Our study provides a quantitative observational estimate of the potential role played by SCVs in the localization of the vertical mixing.

To further assess the potential impact of these local dynamical structures on the deep convection, one has to compare the surface of promoted mixing covered by such SCVs with the total surface of the basin. Again, owing to a hypothetical random presence of about $10 \pm 5$ LIW SCVs over the whole basin, it will represent only 1–3% of its total surface. At the basin scale, the role of the LIW SCVs through their local preconditioning effect is then not a critical trigger for winter vertical mixing. However, they will still have local drastic effects especially in areas of intermediate convection surrounding the DWF zone (like the Ligurian Sea for instance) where the mixed layer typically reaches depths of $\sim$ 500–1000 m in winter. They will also play an important role during weak winters, where vertical mixing could not reach great depths but preferentially only in such dynamical structures.

Finally, these local spots of deep mixing could have important impacts on the local nutrients injection into the euphotic zone. The spring bloom following the winter convective phase generally encompasses a broader surface than the only DWF zone. This could be partially due to the presence of such SCVs that locally favor vertical mixing and consequently the phytoplankton growth, even in areas of weaker mixing than the deep convection area of the Gulf of Lions.

## 5. Summary and Conclusions

In this study, we identified Submesoscale Coherent Vortices (SCV) as key contributors to the spreading of the Levantine Intermediate Waters (LIW) over the whole northwestern Mediterranean Sea (NWMed). Some of them (labeled $L_i^*$) very likely formed from the detachment of the LIW vein flowing along Sardinia, that

might be considered as an undercurrent under upwelling conditions [*Olita et al*., 2013]. In this study, we therefore named this circulation feature the Western Sardinian Undercurrent. Hence, they have very similar formation processes and dynamical similarities to the "Cuddies" (Californian undercurrent eddies) in the North Pacific [*Garfield et al*., 1999; *Pelland et al*., 2013], or subthermocline eddies originating from the Peru-Chile undercurrent [*Johnson and McTaggart*, 2010]. Even though their role and implications are completely different, we propose to analogously name "Suddies" these particular LIW SCVs standing for "Sardinian Undercurrent eddies." The exact role of the mean circulation pattern on the formation of the Suddies is still open and needs to be assessed in order to know whether the NW corner of Sardinia can be considered as the only source of LIW SCVs or not. Consequently, an unknown remains about the exact origin of the SCVs $L_i$ (observed in the central Ligurian Sea) and $G_i$ (observed in the Gulf of Lions). However, the basin-scale implications of the LIW SCVs is still pertinent since all the LIW SCVs share a lot of common characteristics (in particular in terms of heat and salt content anomaly).

The LIW SCVs are made of very warm (+0.2–0.4°C) and saline (+0.07–0.10) LIW compared to the offshore *background* LIW properties and thus carry a great anomaly of heat ($\sim 9\times10^{16}$ J) and salt ($\sim 6\times10^{9}$ kg) toward the basin interior. With a small radius of about 6 km and azimutal peak velocities of about located at intermediate depths ($\sim$ 400m), they are dynamically characterized by a high Rossby number ($\sim$ 0.2–0.3) and a Burger number of $\sim$ 0.5–0.8. It indicates dynamical similarities with other SCVs involved in the spreading of the newly formed Western Mediterranean Deep Waters (WMDW) [*Testor and Gascard*, 2003, 2006]. The open ocean dynamics of the intermediate and deep waters seems therefore to be dominated by such SCVs. It raises modeling issues in order to accurately model these small isolated and long-lived dynamical structures or at least well represent their influence on the large-scale oceanic properties, as well as observational challenges in order to progress in the understanding of the physics of the ocean interior.

The LIW SCVs have certainly strong implications for the basin-scale physics. Indeed, they play an active role in the spreading of the LIW toward the whole NWMed interior through the injection of heat and salt. This is especially important to set the stratification and the hydrographical characteristics of intermediate waters in the Gulf of Lions and the Ligurian Sea before the occurrence of wintertime deep convection events [*Grignon et al*., 2010]. The only transfer of the heat and salt anomaly contained in 1–2 LIW SCVs into the mixed patch during the formation of the WMDW could explain 10–50% of the recurrent trend observed in the WMDW properties since the 1960s [*Bethoux et al*., 1990]. Moreover, as shown by *Schroeder et al*. [2010] and *Herrmann et al*. [2010], the Western Mediterranean Transient (a major production of anomalously warm, salty deep waters in 2005) was caused by the accumulation of heat and salt within the intermediate layers. We discussed the implication of the heat and salt accumulation due to the LIW SCVs during the period of weakly convective winters of the 1990s. In this case, they could have explained a significant part (15–25%) of the observed changes in the deep waters properties. They might therefore have played a crucial role in establishing the favorable conditions prior to this disruption of the WMDW properties with a potential great impact on ocean productivity and the carbon budget of the NWMed. Furthermore, they can greatly influence the deepening of the mixed layer thanks to their weakly stratified core, which makes them more sensitive to winter buoyancy loss. This is particularly critical for the onset of the vertical mixing, as well as the ventilation deep layers during weak winters and in areas of intermediate mixing. Indeed, the mixed layer depth could be greatly enhanced under the influence of such eddies (by a factor of 2), which might have significant impacts on the nutrients input into the euphotic zone and then on the phytoplankton growth.

To our knowledge, SCVs of LIW remained unidentified so far despite a great number of measurements carried out in the relatively small region of the NWMed and the fact that they are recurrent dynamical features. This basin being characterized by a small internal radius of deformation ($\sim$ 5 km) due to its particularly weak stratification, the observation of subthermocline SCVs by other platforms (CTD casts, Argo floats, remote sensing,. . .) was always partial and almost impossible to interpret. The significance of such features could only be revealed by the glider technology providing high-resolution vertical sections on the long term in a framework of sustained basin-scale repeated sections.

At last, as vectors of energy propagation, but also of matter and tracers, the generation of LIW SCVs could also impact the export of dissolved and suspended matter from the continental slope during their formation process. As a matter of fact, they might transport waters characterized by particularly (1) low dissolved oxygen concentrations because of the age of LIW composing their core and (2) lower nutrients

concentration since LIW originates from the ultraoligotrophic eastern Mediterranean Sea characterized by lower nutrients concentration than the western Mediterranean Sea and a different stoichiometry [*Pujo-Pay et al.*, 2011]. The impacts of anticylonic mesoscale eddies on primary production and carbon export in the Mediterranean Sea have been studied for instance by *Moutin and Prieur* [2012], but assessing these crucial questions for such small SCVs is not well known yet and remains a challenge.

## Appendix A : Heat and Salt Content

In order to assess the role of LIW SCVs on the heat and salt injection at intermediate depths, we can estimate the local heat (in J) and salt (in g) content anomalies within each SCV as follows:

$$\Delta HC = \pi \int_{-R}^{R} \epsilon^2 r dr \int_{-1000}^{0} dz \rho(r,z) c_p(S,\theta,p) \Delta\theta(r,z) \quad \text{(A1)}$$

$$\Delta SC = \pi \int_{-R}^{R} \epsilon^2 r dr \int_{-1000}^{0} dz \rho(r,z) \Delta S(r,z) \quad \text{(A2)}$$

where $\Delta\theta(r,z)$ (resp. $\Delta S(r,z)$) represent the radial distribution of the potential temperature (resp. salinity) anomaly compared to the *far-field*, $c_p$ the heat capacity of the seawater and $\rho$ the observed density. The integration is performed between the surface and a depth of 1000 m on the vertical, and over a radial distance encompassing the $\theta/S$ anomaly of the SCVs. The results of this integration for the different SCVs ($L_i^*$, $G_i$ and $L_i$) are summarized in Table 2. We end up with a mean heat and salt content for the SCVs $L_i^*$ and $L_i$ observed in the Ligurian Sea of $(8.4 \pm 6.5)\times10^{16}$ J and $(5.6 \pm 3.7)\times10^{9}$ kg. Since the background LIW properties are less marked in Gulf of Lions area (see Figure 1), the LIW SCVs $G_i$ observed there transport a heat/salt anomaly of the same order of magnitude: $(8.7 \pm 4.7)\times10^{16}$ J and $(5.9 \pm 3.1)\times10^{9}$ kg.

## Appendix B : Stratification Effects

Because SCVs have a low stratified core, they can help the deepening of the mixed layer. To quantify this aspect, we compute the columnar buoyancy, *IS*(*z*) (corresponding to a stratification index). This quantity is also equal to the total buoyancy flux required to mix an initially stratified water column down to the depth *z* [*Herrmann et al.*, 2008]:

$$IS(z) = \int_0^z N^2(Z) Z dZ = \int B_s(t) dt \quad \text{(B1)}$$

where $B_s(t)$ is the surface buoyancy loss.

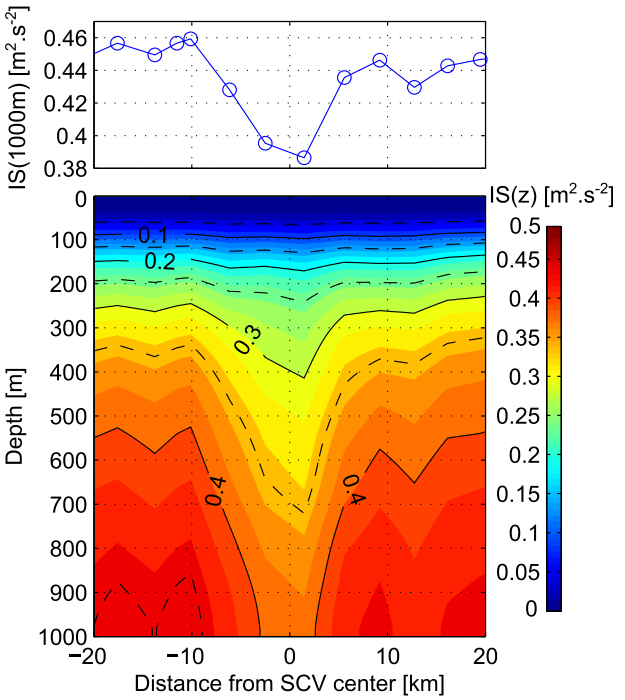


**Figure B1.** (bottom) Columnar buoyancy across the SCV $L_2^*$ (see Figure 2). (top) Buoyancy loss required to mix the water column down to 1000 m.

The Figure B1 illustrates the case of SCV $L_2^*$ observed in November 2010. The presence of this LIW SCV results in a buoyancy flux decrease of about 0.07 $m^2\ s^{-2}$ in order to mix the water column down to 1000m in the center of the SCV compared to the surroundings. Comparing this quantity to the absolute value of the columnar buoyancy ($IS(1000\ m) \sim 0.45\ m^2\ s^{-2}$, typical values for the pre-winter stratification), the reduction represents about 15% of the required buoyancy loss. It is also comparable to about the buoyancy loss of a winter storm, which typically peaks at $\sim 3.0 \times10^{-7}\ m^2\ s^{-3}$ (see Figure 7 in *Herrmann et al.* [2010]) and persists for about a week, resulting in an integrated buoyancy loss of $\sim 0.08\ m^2\ s^{-2}$.

Gliders cannot provide informations on the lower part of the SCVs, so it is speculative to conclude about their effect on the total columnar buoyancy of the water column. Besides, SCVs might not be able to survive once the vertical mixing has reached their core. However, the local reduction of the columnar buoyancy (within the first 1000m) can be significant for the onset of the convection, being equivalent to about the effect of a winter storm on the columnar buoyancy of the upper part of the water column.

**Acknowledgments**
GlobColour has been originally funded by ESA with data from ESA, NASA, NOAA, and GeoEye. This reprocessing version has received funding from the European Community's Seventh Framework programme (FP7/2007–2013) under grant agreement 282723 (OSS2015 project). The hydrographical data were collected and made freely available by the Coriolis project and programmes that contribute to it (http://www.coriolis.eu.org). We would like to acknowledge the technical staff of the DT-INSU for logistic and technical support for the gliders deployments. Captains, crew members of R/V *Le Tethys II* (INSU), and *Le Suroit* (Ifremer), as well as scientists who participated to the MOOSE-GE, DEWEX, and DOWEX different cruises are also warmly thanked. Support was provided by the French MISTRALS program (HyMeX and MERMeX components) and MOOSE project (AllEnvi-INSU long-term observatory), and the FP7 EU projects GROOM (grant agreement 284321), PERSEUS (grant agreement 287600), and JERICO (grant agreement 262584) as well as the EGO-COST Action ES0904. A. Bosse was funded by a French government scholarship.

## References

Albérola, C., C. Millot, and J. Font (1995), On the seasonal and mesoscale variabilities of the Northem Current during the PRIM0-0 experiment in the western Mediterranean Sea, *Oceanol. Acta*, *18*, 163–192.
Allen, S. E. (2000), On subinertial flow in submarine canyons: Effect of geometry, *J. Geophys. Res.*, *105*, 1285–1297.
Armi, L., D. Hebert, N. Oakey, J. Price, P. L. Richardson, T. Rossby, and B. a. Ruddick (1988), The history and decay of a Mediterranean salt lens, *Nature*, *333*, 649–651.
Benthuysen, J., and L. N. Thomas (2012), Friction and diapycnal mixing at a slope: Boundary control of potential vorticity, *J. Phys. Oceanogr.*, *42*, 1509–1523.
Bethoux, J.-P., B. Gentili, J. Raunet, and D. Tailliez (1990), Warming trend in the western Mediterranean deep water, *Nature*, *347*, 660–662.
Boehme, L., and U. Send (2005), Objective analyses of hydrographic data for referencing profiling float salinities in highly variable environments, *Deep Sea Res. Part II*, *52*, 651–664.
Bouffard, J., A. Pascual, S. Ruiz, Y. Faugère, and J. Tintoré (2010), Coastal and mesoscale dynamics characterization using altimetry and gliders: A case study in the Balearic Sea, *J. Geophys. Res.*, *115*, C10029, doi:10.1029/2009JC006087.
Carnevale, G., R. Kloosterzielz, and G. van Heijst (1991), Propagation of barotropic vortices over topography in a rotating tank, *J. Fluid Mech.*, *233*, 119–139.
Cushman-Roisin, B., E. Chassignet, and B. Tang (1990), Westward motion of mesoscale eddies, *J. Phys. Oceanogr.*, *20*, 758–768.
D'Asaro, E. A. (1988), Generation of submesoscale vortices: A new mechanism, *J. Geophys. Res.*, *93*, 6685–6693.
Davis, R. E., W. S. Kessler, and J. T. Sherman (2012), Gliders measure Western Boundary current transport from the South Pacific to the Equator, *J. Phys. Oceanogr.*, *42*, 2001–2013.
Dewar, W. K., and H. Meng (1995), The propagation of submesoscale coherent vortices, *J. Phys. Oceanogr.*, *25*, 1745–1770.
Durrieu de Madron, X., et al. (2013), Interaction of dense shelf water cascading and open-sea convection in the northwestern Mediterranean during winter 2012, *Geophys. Res. Lett.*, *40*, 1379–1385, doi:10.1002/grl.50331.
Elliott, B. A., and T. B. Sanford (1986), The subthermocline lens D1. Part II: Kinematics and dynamics, *J. Phys. Oceanogr.*, *16*, 549–561.
Garau, B., S. Ruiz, W. G. Zhang, A. Pascual, E. Heslop, J. Kerfoot, and J. Tintoré (2011), Thermal lag correction on slocum CTD glider data, *J. Atmos. Oceanic Technol.*, *28*, 1065–1071, doi:10.1175/JTECH-D-10–05030.1.
Garfield, N., C. Collins, R. Paquette, and E. Carter (1999), Lagrangian exploration of the California undercurrent, 1992–1995, *J. Phys. Oceanogr.*, *29*, 560–583.
Gascard, J.-C. (1978), Mediterranean deep water formation baroclinic instability and oceanic eddies, *Oceanol. Acta*, *1*, 315–330.
Gascard, J.-C., A. J. Watson, M.-J. Messias, K. A. Olsson, T. Johannessen, and K. Simonsen (2002), Long-lived vortices as a mode of deep ventilation in the Greenland Sea, *Nature*, *416*, 525–1527.
Gasparini, G., A. Ortona, G. Budillon, M. Astraldi, and E. Sansone (2005), The effect of the Eastern Mediterranean Transient on the hydrographic characteristics in the Strait of Sicily and in the Tyrrhenian Sea, *Deep Sea Res. Part I*, *52*, 915–935,.
Gourdeau, L., W. S. Kessler, R. E. Davis, J. Sherman, C. Maes, and E. Kestenare (2008), Zonal Jets entering the coral sea, *J. Phys. Oceanogr.*, *38*, 715–725.
Grignon, L., D. A. Smeed, H. L. Bryden, and K. Schroeder (2010), Importance of the variability of hydrographic preconditioning for deep convection in the Gulf of Lion, NW Mediterranean, *Ocean Sci.*, *6*, 573–586.
Herrmann, M., S. Somot, F. Sevault, C. Estournel, and M. Déqué (2008), Modeling the deep convection in the northwestern Mediterranean Sea using an eddy-permitting and an eddy-resolving model: Case study of winter 1986–1987, *J. Geophys. Res.*, *113*, C04011, doi:10.1029/2006JC003991.
Herrmann, M., F. Sevault, J. Beuvier, and S. Somot (2010), What induced the exceptional 2005 convection event in the northwestern Mediterranean basin? Answers from a modeling study, *J. Geophys. Res.*, *115*, C12051, doi:10.1029/2010JC006162.
Houpert, L. (2003), Contribution to the study of transfer processes from the surface to the deep ocean in the Mediterranean sea using in situ measurements, PhD thesis, Univ. de Perpignan, Perpignan, France.
Høydalsvik, F., C. Mauritzen, K. Orvik, J. LaCasce, C. Lee, and J. Gobat (2013), Transport estimates of the western branch of the Norwegian Atlantic current from glider surveys, *Deep Sea Res. Part I*, *79*, 86–95.
Johnson, G. C., and K. E. McTaggart (2010), Equatorial Pacific 13°C water eddies in the eastern subtropical south Pacific Ocean, *J. Phys. Oceanogr.*, *40*, 226–236.
Lacombe, H., P. Tchernia, and L. Gamberoni (1985), Variable bottom water in the western Mediterranean basin, *Prog. Oceanogr.*, *14*, 319–338.
Lascaratos, A., W. Roether, K. Nittis, and B. Klein (1999), Recent changes in deep water formation and spreading in the eastern Mediterranean Sea: A review, *Prog. Oceanogr.*, *44*, 5–36.
Legg, S., J. M. Williams, and J. Gao (1998), Localization of deep ocean convection by a mesoscale eddy, *J. Phys. Oceanogr.*, *28*, 944–970.
Lherminier, P., J.-C. Gascard, and D. Quadfasel (1999), The Greenland Sea in water 1993 and 1994: Preconditioning for deep convection, *Deep Sea Res., Part II*, *46*, 1199–1235.
Madec, G., F. Lott, P. Delecluse, and M. Crépon (1996), Large-scale preconditioning of deep-water formation in the northwestern Mediterranean sea, *J. Phys. Oceanogr.*, *26*, 1393–1408.
Malanotte-Rizzoli, P., B. B. Manca, M. R. d'Alcala, A. Theocharis, S. Brenner, G. Budillon, and E. Ozsoy (1999), The eastern Mediterranean in the 80s and in the 90s: The big transition in the intermediate and deep circulations, *Dyn. Atmos. Oceans*, *29*, 365–395.
Mancho, A. M., E. Hernandez-Garcia, D. Small, S. Wiggins, and V. Fernandez (2008), Lagrangian transport through an ocean front in the northwestern Mediterranean sea, *J. Phys. Oceanogr.*, *38*, 1222–1237.
Marshall, D. P., and C. E. Tansley (2001), An implicit formula for boundary current separation, *J. Phys. Oceanogr.*, *31*, 1633–1638.
Marshall, J., and F. Schott (1999), Open-ocean convection: Observations, theory, and models, *Rev. Geophys.*, *37*, 1–64.
McWilliams, J. C. (1985), Submesoscale, coherent vortices in the ocean, *Rev. Geophys.*, *23*, 165–182.

McWilliams, J. C. (1988), Vortex generation through balanced adjustment, *J. Phys. Oceanogr.*, *18*, 1178–1192.
MEDOC-Group (1970), Observation of formation of deep water in the Mediterranean sea, 1969, *Nature*, *225*, 1037–1040.
Millot, C. (1987), The circulation of the Levantine intermediate water in the Algerian basin, *J. Geophys. Res.*, *92*, 8265–8276.
Millot, C. (1999), Circulation in the western Mediterranean sea, *J. Mar. Syst.*, *20*, 423–442.
Millot, C., and I. Taupier-Letage (2005), Additional evidence of LIW entrainment across the Algerian subbasin by mesoscale eddies and not by a permanent westward flow, *Prog. Oceanogr.*, *66*, 231–250.
Millot, C., I. Taupier-Letage, and M. Benzohra (1990), The Algerian eddies, *Earth Sci. Rev.*, *27*, 203–219.
Molemaker, M. J., J. McWilliams, and W. K. Dewar (2014), Submesoscale instability and generation of mesoscale anticyclones near a separation of the California undercurrent, *J. Phys. Oceanogr.*, doi:10.1175/JPO-D-13-0225.1.
Moutin, T., and L. Prieur (2012), Influence of anticyclonic eddies on the biogeochemistry from the oligotrophic to the ultraoligotrophic Mediterranean (BOUM cruise), *Biogeosciences*, *9*, 3827–3855, doi:10.5194/bg-9–3827-2012.
Niewiadomska, K., H. Claustre, L. Prieur, and F. D'Ortenzio (2008), Submesoscale physical-biogeochemical coupling across the Ligurian current (northwestern Mediterranean) using a bio-optical glider, *Limnol. Oceanogr.*, *53*, 2210–2225.
Noble, M. A., and S. R. Ramp (2000), Subtidal currents over the central California slope: Evidence for offshore veering of the undercurrent and for direct, wind-driven slope currents, *Deep Sea Res. Part II 47*, 871–906.
Olita, A., A. Ribotti, L. Fazioli, A. Perilli, and R. Sorgente (2013), Surface circulation and upwelling in the western Sardinia sea: A numerical study, *Cont. Shelf Res.*, *71*, 95–108, doi:10.1016/j.csr.2013.10.011.
Pelland, N. A., C. C. Eriksen, and C. M. Lee (2013), Subthermocline eddies over the Washington Continental slope as observed by seagliders, 2003-09, *J. Phys. Oceanogr.*, *43*, 2025–2053.
Piccioni, A., M. Gabriele, E. Salusti, and E. Zambianchi (1988), Wind-induced upwellings off the southern coast of Sicily, *Oceanol. Acta*, *11*, 309–321.
Pietri, A., P. Testor, V. Echevin, A. Chaigneau, L. Mortier, G. Eldin, and C. Grados (2013), Finescale vertical structure of the upwelling system off southern Peru as observed from glider data, *J. Phys. Oceanogr.*, *43*, 631–646.
Pietri, A., V. Echevin, P. Testor, A. Chaigneau, L. Mortier, C. Grados, and A. Albert (2014), Impact of a coastal-trapped wave on the near-coastal circulation of the Peru upwelling system from glider data, *J. Geophys. Res. Oceans*, *119*, 2109–2120, doi:10.1002/2013JC009270.
Pinardi, N., et al. (2013), Mediterranean Sea large-scale low-frequency ocean variability and water mass formation rates from 1987 to 2007: A retrospective analysis, *Prog. Oceanogr.*, in press, doi:10.1016/j.pocean.2013.11.003. [Available at http://www.sciencedirect.com/science/article/pii/S007966111300222X.]
Poulain, P.-M., M. Menna, and E. Mauri (2012), Surface geostrophic circulation of the Mediterranean sea derived from drifter and satellite altimeter data, *J. Phys. Oceanogr.*, *42*, 973–990.
Pujo-Pay, M., P. Conan, L. Oriol, V. Cornet-Barthaux, C. Falco, J.-F. Ghiglione, C. Goyet, T. Moutin, and L. Prieur (2011), Integrated survey of elemental stoichiometry (C, N, P) from the western to eastern Mediterranean sea, *Biogeosciences*, *8*, 883–899.
Robinson, A., and M. Golnaraghi (1994), The physical and dynamical oceanography of the Mediterranean sea, in *Ocean Processes in Climate Dynamics: Global and Mediterranean Examples, NATO ASI Ser.*, vol. 419, edited by P. Malanotte-Rizzoli and A. Robinson, pp. 255–306, Springer, Netherlands.
Schroeder, K., G. P. Gasparini, M. Tangherlini, and M. Astraldi (2006), Deep and intermediate water in the western Mediterranean under the influence of the eastern Mediterranean transient, *Geophys. Res. Lett.*, *33*, L21607, doi:10.1029/2006GL027121.
Schroeder, K., A. Ribotti, M. Borghini, R. Sorgente, A. Perilli, and G. Gasparini (2008), An extensive western Mediterranean deep water renewal between 2004 and 2006, *Geophys. Res. Lett.*, *35*, L18605, doi:10.1029/2008GL035146.
Schroeder, K., S. A. Josey, M. Herrmann, L. Grignon, G. P. Gasparini, and H. L. Bryden (2010), Abrupt warming and salting of the western Mediterranean deep water after 2005: Atmospheric forcings and lateral advection, *J. Geophys. Res.*, *115*, C08029, doi:10.1029/2009JC005749.
Stommel, H., H. Bryden, and P. Mangelsdorf (1973), Does some of the Mediterranean outflow come from great depth?, *Pure Appl. Geophys.*, *105*, 879–889.
Testor, P., and J.-C. Gascard (2003), Large-scale spreading of deep waters in the western Mediterranean sa by submesoscale coherent eddies, *J. Phys. Oceanogr.*, *33*, 75–87.
Testor, P., and J.-C. Gascard (2005), Large scale flow separation and mesoscale eddy formation in the Algerian Basin, *Prog. Oceanogr.*, *66*, 211–230.
Testor, P., and J.-C. Gascard (2006), Post-convection spreading phase in the northwestern Mediterranean sea, *Deep Sea Res. Part I*, *53*, 869–893.
Testor, P., K. Béranger, and L. Mortier (2005a), Modeling the deep eddy field in the southwestern Mediterranean: The life cycle of Sardinian eddies, *Geophys. Res. Lett.*, *32*, L13602, doi:10.1029/2004GL022283.
Testor, P., U. Send, J.-C. Gascard, C. Millot, I. Taupier-Letage, and K. Béranger (2005b), The mean circulation of the southwestern Mediterranean sea: Algerian Gyres, *J. Geophys. Res.*, *110*, C11017, doi:10.1029/2004JC002861.
Testor, P., et al. (2010), Gliders as a component of future observing systems, in *Proceedings of OceanObs'09: Sustained Ocean Observations and Information for Society (Vol. 2), Venice, Italy, 21–25 September 2009*, edited by J. Hall, D. E. Harrison and D. Stammer, 1021–1038, doi:10.5270/OceanObs09.cwp.89.
Todd, R. E., D. L. Rudnick, and R. E. Davis (2009), Monitoring the greater San Pedro Bay region using autonomous underwater gliders during fall of 2006, *J. Geophys. Res.*, *114*, C06001, doi:10.1029/2008JC005086.
van Haren, H., M. Ribò, and P. Puig (2013), (Sub-)inertial wave boundary turbulence in the Gulf of Valencia, *J. Geophys. Res. Oceans*, *118*, 2067–2073, doi:10.1002/jgrc.20168.
Vandermeirsch, F., Y. Morel, and G. Sutyrin (2001), The net advective effect of a vertically sheared current on a coherent vortex, *J. Phys. Oceanogr.*, *31*, 2210–2225.